Drug Delivery and Translational Research (2022) 12:1659–1683
https://doi.org/10.1007/s13346-021-01058-6

ORIGINAL ARTICLE

In vitro release, ex vivo penetration, and in vivo dermatokinetics of ketoconazole-loaded solid lipid nanoparticles for topical delivery

Mohhammad Ramzan[1] · Samuel Gourion-Arsiquaud[2] · Afzal Hussain[3] · Jaspreet Singh Gulati[4] · Qihong Zhang[2] · Sonia Trehan[5] · Vinam Puri[5] · Bozena Michniak-Kohn[5] · Indu Pal Kaur[1]

Accepted: 28 August 2021 / Published online: 7 January 2022

Abstract

The study focused to evaluate and investigate optimized (using QbD) and novel ketoconazole (KTZ)-loaded solid lipid nanoparticles (KTZ-SLNs; 2% w/v KTZ) for enhanced permeation across skin. KTZ-SLNs were evaluated for size, distribution, zeta potential (ZP), percent entrapment efficiency (%EE), drug release, morphology (HRTEM and FESEM), thermal behaviour (DSC), spectroscopic (FTIR), and solid-state/diffraction characterization (X-ray diffraction, XRD). Moreover, ex vivo permeation and drug deposition into rat skin were conducted using Franz diffusion cell. The same was confirmed using human dermatome skin and fluorescence, confocal Raman, and vibrational ATR-FTIR microscopic methods. An in vivo dermatokinetics study was performed in rats to assess the extent of KTZ permeation into the skin. Stability including accelerated and photostability studies were conducted at different temperatures (2–8, 30, and 40 °C) for 12 months. The spherical, optimized KTZ-SLN formulation (KOF1) showed particle size of 293 nm and high EE of 88.5%. Results of FTIR, DSC, and XRD confirmed formation of KTZ-SLNs and their amorphous nature due to presence of KTZ in a dissolved state in the lipid matrix. In vitro release was slow and sustained whereas ex vivo permeation parameters were significantly high in KTZ-SLNs as compared to free drug suspension (KTZ-SUS) and marketed product (Nizral®; 2% KTZ w/v). Drug retention was 10- and five-fold higher than KTZ-SUS and marketed product, respectively. In vivo dermatokinetics parameters improved significantly with SLN formulation (410–900% enhanced). Confocal Raman spectroscopy experiment showed that KTZ-SLNs could penetrate beyond the human stratum corneum into viable epidermis. Fluorescent microscopy also indicated improved penetration of KTZ-SLNs. KTZ-SLNs were photostable and showed long-term stability over 12 months under set conditions.

Keywords Design Expert · Imaging studies · ATR-FTIR studies · Skin bioavailability · Antifungals · Skin fungal infection

Introduction

Superficial and deep cutaneous fungal infections are common worldwide and constitute one-fourth of common skin infections caused by dermatophytes [1]. The dermatophytes tend to invade the keratinized tissue of stratum corneum (SC) and cause dermal seborrheic dermatitis followed by severe psychological, social, and financial consequences for patients [1, 2]. Most fungal infections survive in the lower epidermal (stratum basale layer) [2], superficial region, and the vellus hairs [3, 4]. Most fungal cells have specialized efflux system resulting in frequent drug resistance [5]. Sub-optimal concentration at the site of infection, poor compliance to therapy, and poor delivery modalities, and active efflux system result in frequent recurrence, chronic infections, and serious drug resistance development. Dermatophyte-mediated intracellular infections are critical to treat due to long-term therapy and patient non-compliance using conventional dosage form [6]. These sites are poorly accessible to the conventional formulations resulting in challenged therapeutic efficacy.

Ketoconazole (KTZ) is a broad-spectrum, antifungal agent clinically recommended to control cutaneous fungal

✉ Indu Pal Kaur
indupalkaur@yahoo.com; dripkuips@gmail.com

[1] Department of Pharmaceutics, University Institute of Pharmaceutical Sciences, Panjab University, Sector 14, Chandigarh 160014, India

[2] TRI Princeton, Princeton, NJ 08540, USA

[3] Department of Pharmaceutics, College of Pharmacy, King Saud University, Riyadh 11451, Saudi Arabia

[4] Hitech Formulations Pvt. Ltd., Chandigarh 160002, India

[5] Center for Dermal Research, Rutgers University, Piscataway, NJ 08854, USA

infections (candidiasis, tinea, and related skin fungal infections). The drug has a potential to control cutaneous superficial (*Candida* and *Malassezia*), localized, and secondary infections such as androgenic alopecia, *leishmaniasis*, and yeast-induced blepharitis [6]. Pharmaceutically, KTZ is a lipophilic drug (log $P = 4.74$), with poor aqueous solubility (0.04 mg/mL) and light sensitivity, and it is challenging to formulate it into an efficient topical product with promising therapeutic efficacy across the SC barrier [7]. KTZ is associated with several undesirable effects (nausea, vomiting, gastrointestinal disturbance, and hepatotoxicity) after oral administration [8]. Likewise, conventional creams are associated with limited drug access to the target site, side effects (swelling, irritation/redness, itching, and contact dermatitis), and poor therapeutic efficacy to control deeper skin infections [9]. Improved permeability/availability at sites of infection including vellus hair and viable epidermis and dermis coupled with a slow-controlled release which can manage side effects is thus desired for KTZ. All of this can be addressed using nanocarrier systems for delivering KTZ.

To manage these issues, KTZ has been formulated in various novel nanocarriers like transethosomes [9], ethosomes [10], nanoemulgel [11], biocompatible water-cosolvent binary mixtures [12], lipidic nanocarriers (solid lipid nanoparticles as SLNs and nanostructured lipid carriers as NLCs) [13], and liposomes [14]. However, these reports achieved limited drug loading and inefficient permeation across rat skin. Drug loading is defined as the amount of drug present per unit of the matrix (lipid in the case of SLNs). Furthermore, in spite of substantial data on in vitro or antifungal activity of KTZ or its nanoformulations, most studies do not document any significant in vivo pharmacokinetic data establishing superiority of the product. Moreover, retained organic solvents in the final product of several of these reported approaches challenge the safety of topical formulations. Considering these contexts, we sequentially conducted in vitro release, ex vivo permeation, in vivo dermatokinetic and skin penetration studies on KTZ-SLNs to offer a complete proof of concept for the treatment of fungal infections surviving even in the deeper dermal sites of skin. This is a first report describing dermatokinetics of optimized (using QbD) SLNs of KTZ prepared using a high-pressure homogenization (HPH) method without employing any toxic solvent. Moreover, ex vivo data (extent of permeation and drug retention) in rat skin is corroborated with spectroscopic (confocal Raman and ATR-FTIR imaging) and fluorescence probe labelled studies in human dermatome skin. Use of vibrational spectroscopic and fluorescence microscopic methods to explore penetration of a SLN formulation in skin described here is also unique to this study and a less explored, though a reliable approach [15, 16]. Rat skin is though considered as a good surrogate for human skin, but we thought it appropriate to confirm permeation in human skin following promising results with rat skin. Earlier, we have established improved antifungal efficacy (MIC), cellular uptake (both into dermal fibroblasts and *Candida* cells), and multitier in vitro and in vivo safety of KTZ-SLNs described herein [17].

Thus, the present study was designed comprehensively to rationalize improved efficacy of SLNs ferrying KTZ. SLN formulation is highly suitable for lipophilic actives like KTZ and is expected to result in remarkable clinical benefits over conventional dosage forms via (a) alleviated permeation following application; (b) nanoscale particles are retained in the form of a depot in the follicles and vellus hair [18] for slow and sustained delivery in the region to manage relapse; (c) lipid-based nanocarriers exhibit augmented cellular internalization within fibroblasts (seat of infection) and fungal strains, as already established for presently reported KTZ-SLNs [17]; (d) substantial and constant exposure of the fungal load to KTZ laden SLNs due to controlled release effect; (e) latter will also ensure lesser or no side effects; (f) resulting in improved therapeutic efficacy with high patient compliance [12, 13, 19–21].

SLNs are a well explored system to improve solubility and therapeutic efficacy of several potential antifungal agents. We have earlier reported improved ocular delivery for KTZ-SLNs with a drug loading of 8% w/v whereas Souto et al. report a drug loading in the range of 5.1–7.4% w/w [13, 20]. Similarly, most of the previously published work reports ~1% (w/v) or less concentration of KTZ in the SLN dispersion [21]. In the present study, we ventured to develop a (i) 2% w/v KTZ formulation to match the strength of marketed product (Nizral® 2% w/v; Jenssen Pharmaceuticals), (ii) with a higher drug loading of 20% w/w with respect to the lipid matrix (as indicated above it is a theoretical value obtained from drug to the lipid ratio employed in the SLN composition), which will (iii) penetrate the SC and reach deeper epidermal and dermal regions (iv) and release KTZ over sufficient period and in enough quantity to manage infection and related issues of relapse and resistance. We have earlier established a significant reduction of 4–83 times in MIC of KTZ upon incorporation into SLNs against an array of fungal strains including two resistant strains [17]. The enhanced effect was attributed to facilitated permeation of KTZ across the fungal cell walls, its accumulation to the toxic level in the fungal cell and increased cellular interaction after loading into SLNs [22]. Thus, the presently described and explored KTZ-SLN formulation optimized using design of experiment (DoE/QbD) for high drug loading and entrapment efficiency coupled with suitably small size is associated with controlled release, economic cost, and feasibility for scale up for large-scale production. The adopted HPH method of preparing KTZ-SLN formulation is scalable and the formulation has obvious benefits of increased drug solubility in lipid matrix, biocompatibility, drug protection (stability and photostability), optimized drug loading, and optimized process

variables [23]. It may also be noted that KTZ-SLN compositions described herein are novel and patented [24].

In this study, we optimized KTZ-loaded SLN formulation using experimental design tool and characterized it for in vitro parameters (particle size, size distribution, shape, zeta potential, solid-state properties, and in vitro drug release). Moreover, the optimized formulation was studied for ex vivo (rat skin and human dermatome skin) and in vivo pharmacokinetic performance in rat model. Long-term stability study at different temperatures and photo-stability ensured the success of the product over a period of 1 year.

Materials

Ketoconazole (KTZ > 99.5% pure, AR grade) was procured from a local pharmaceutical industry (Velite Pharmaceuticals, Ludhiana, Punjab, India). Phospholipon 90G (P 90G) and Compritol 888 ATO (CATO) were obtained as gift samples from Lipoid (Germany) and Gattefosse (France), respectively. Polyethylene glycol 400 (as cosolvent) and tween 80 (as surfactant) were procured from CDH, Mumbai (India). Millipore water was used as aqueous solvent wherever required in the study. Fluorescence dye (fluorescein sodium) was purchased from Sigma-Aldrich (Mumbai, India). All chemicals were of analytical grade.

Methods

Preliminary screening studies

Several batches of blank formulations were prepared to screen excipients such as solid lipid (Compritol® 888 ATO), surfactant (tween 80), cosolvent (polyethylene glycol 600) (PEG 600), and stabilizer (Phospholipon 90 G) (P 90G). Taguchi design was applied for factors and levels. Several variables (run cycles, speed, and stirring time) of high-pressure homogenization (HPH) technique were optimized to get stable SLNs (overnight benchtop stability).

Formulation method to load KTZ in solid lipid nanoparticles (KTZ-SLNs)

A preliminary study was carried out to select excipients and their levels (low and high). Based on benchtop stable product, the higher and the lower levels of factors were decided to feed as input parameters in experimental design software (Design Expert). The lipid organic phase was composed of CATO, PEG-600, and KTZ (fixed amount) which was heated to melt at 75 °C. Similarly, the aqueous phase contained tween 80 and P90G previously set at the same temperature. The aqueous phase was stirred at high speed (1000 rpm) using a stirrer (WiseTis, HG-15D, Daihan, Korea). The hot organic phase was slowly added to the aqueous phase under constant stirring to result in a coarse emulsion. The prepared coarse emulsion was passed through a high-pressure homogenizer (HPH) (EmulsiFlex-C3, Avestin, Canada), at 1000 bar pressure for 7 cycles. The formed o/w emulsion was cooled to room temperature to achieve KTZ-loaded SLNs (2% w/v). Thus, several batches of formulations were formulated as dictated in experimental design (central composite design). In the case of fluorescein sodium dye–probed SLNs (FL-SLNs), the same procedure was adopted except that the dye was dissolved in aqueous phase. Free fluorescein was removed from the system by dialysis against water for 1h prior to application.

Optimization process

Experimental protocol was designed to evaluate the critical factors and their significant levels to get the most robust formulation with optimal content of lipid (CATO) and tween 80 (surfactant). A central composite design (CCD) with $\alpha = 1.414$ was run in the Design Expert® (version 8.0.1 Stat-Ease Inc. USA). CATO (X_1) and tween 80 (X_2) were selected as independent variables (factors). Similarly, mean particle size (Y_1), %EE (Y_2), and total drug content (Y_3) were responses (dependent variables). In optimization process, total 13 runs were experimented at 5 levels ($-\alpha, -1, 0, +1, +\alpha$). A general polynomial mathematical quadratic equation was generated to quantify and establish a correlation between the independent (X) and dependent variables (Y):

$$\mathbf{Y} = \boldsymbol{\beta}_0 + \boldsymbol{\beta}_1 \boldsymbol{X}_1 + \boldsymbol{\beta}_2 \boldsymbol{X}_2 + \boldsymbol{\beta}_3 \boldsymbol{X}_1 \boldsymbol{X}_2 + \boldsymbol{\beta}_4 \boldsymbol{X}_2^{\,2} + \boldsymbol{\beta}_5 \boldsymbol{X}_2^{\,2}$$

where Y is dependent variable with two coefficients (β_1 and β_2) of factors (X_1 and X_2). β_0 is an intercept. β_3 is a coefficient of interaction between factors X_1 and X_2, whereas β_4 and β_5 are the coefficients of quadratic terms "X_1" and "X_2", respectively. Positive and negative signs indicate synergistic and antagonistic effect of factors on the response, respectively. ANOVA (analysis of variance) provides parameters (F, p, and r^2 values) to validate the model applied for optimization process using the experimental design.

Characterization of KTZ-loaded SLN formulations

Measurement of particle size, polydispersity index, and zeta potential

Particle size, size distribution, and surface charge are critical factors to control in vitro and in vivo performance of any product. Particle size and PDI were measured using a photon correlation spectroscopy (PCS) technique which is based on the principle of light diffraction phenomenon. The sample was previously diluted with water (50-fold) for analysis (Beckman Coulter, Delsa™ Nano C, USA). Zeta potential of KTZ-SLNs dispersion was measured without sample dilution

(Beckman Coulter, Delsa™ Nano C zetasizer, USA) at 25 °C and the electric field strength of 23.2 V/cm. Experiments were replicated for mean and standard deviation ($n = 3$).

Drug assay/total drug content (%TDC) and entrapment efficiency (%EE)

Formulation (1 g) was dissolved in chloroform:methanol mixture (2:1). The mixture of organic solvents was able to dissolve and disrupt solid lipid of tailored KTZ-SLNs. The mixture was filtered and the content of KTZ was quantified using a validated HPLC method. %EE was determined by dialyzing KTZ-SLN dispersion (1 mL) in a semi-permeable dialysis membrane (12 K Dalton molecular weight cut-offs, HiMedia, Laboratories, Pvt., Mumbai, India) immersed in 50 mL ethanol and stirred magnetically. After 1h, KTZ-SLNs were removed from the bag, disrupted with suitable quantity of chloroform:methanol mixture (2:1), and the amount of drug was determined by HPLC. The dialysate was decided based on the assumption that the entire quantity of unentrapped drug can dissolve in a suitable quantity (50 mL) in an appropriate time (< 1h) to accurately determine the amount of unentrapped drug. The experiment was replicated for mean and standard deviation values ($n = 3$).

$$\text{Total drug content}(\%\ \text{w/w}) = \frac{\text{Drug present in the formulation}}{\text{Total content of formulation}} \times 100$$

%EE was calculated using the following formula:

$$\%\text{EE}(\%\ \text{w/w}) = \frac{\text{Initial drug content} - \text{Free drug content}}{\text{Initial drug content}} \times 100$$

Desirability function

The desirability parameter was used to identify and evaluate the optimized formulation by experimental design. Mathematically, this is a numerical function parameter to identify possible interaction between factors. Moreover, it depends upon the set conditions of optimization process such as goal and importance given to each dependent and independent variable. The value of desirability function varies from zero to unity. Zero indicates the model is not fit and out of optimization whereas the value approaching unity indicates the best fit of the model applied for optimization. The significant terms ($p < 0.05$) were chosen for final equations. The model was considered to be the best fit when the actual correlation coefficient (r^2) value was close to the adjusted correlation coefficient (adjusted r^2). Selected formulations of KTZ-SLNs were prepared from the design space and used as checkpoints to assess the prognostic behaviour of the developed mathematical model.

Preparation of KTZ suspension (KTZ-SUS)

KTZ suspension (KTZ-SUS) was prepared by the method described before with slight modification [20]. An accurately weighed amount of KTZ was dispersed in water containing 1% w/v of tween 80 as surfactant and sodium salt of carboxy methyl cellulose (0.1%w/v) as suspending agent. The drug was rigorously stirred for 60 min in the aqueous phase to obtain a stable suspension with optimal consistency. Final strength of the suspension was equivalent to commercial product (2%w/v). This product was used in the further studies as control.

Lyophilization of KTZ-SLNs

Water must be removed from the aqueous KTZ-SLN dispersion to form a dry and free-flowing powder for Fourier transform infrared spectroscopy (FTIR) and powder X-ray diffraction (PXRD) studies. The formulations (KTZ-SLNs and blank SLNs) were lyophilized in a freeze dryer (Freeze-dryer Alpha 1–2 LD plus, Martin Christ, Germany) without any other additive or cryoprotectant. PEG 600 present in the formulation acts as a suitable cryoprotectant. The KTZ-SLNs and blank SLNs were frozen keeping the sample overnight in the freezer, 1 day before the start of the process, vacuum was applied, and the frozen samples were subjected to drying phase for 12h to get the lyophilized KTZ-SLN product.

Thermal behaviour of the formulations

The thermal behaviour (fusion temperature and fusion enthalpy) of pure KTZ and optimized KTZ-SLN formulation (KOF1) were assessed using a differential scanning calorimeter (DSC). A weighed amount (2 mg) of the lipid, KTZ, PEG 600, P 90G, KTZ-SLNs, or blank SLNs, respectively, were placed in an aluminium pan and heated at a fixed heating rate (10 °C/min) until 300 °C using DSC (821e Mettler Toledo, Switzerland). The generated thermograms were analysed and marked for the values of any significant shift or disappearance/appearance of new peaks. The calorimeter was calibrated by pure indium (melting point) for nitrogen flow and heating rate. Nitrogen gas was used at a purging rate of 50 mL/min.

Fourier transform infrared (FTIR)

Free pristine KTZ, lyophilized KOF1 and blank SLNs were subjected to FTIR analysis. The FTIR spectrometer (Agilent Technologies 630 Cary) was run for the sample using a disc method. A small amount of the sample was physically mixed with KBr followed by disc formation. The disc was

processed for characteristic peaks using Micro Lab software. The samples were scanned over the range of 4000–400 cm^{-1}.

Powder X-ray diffraction (XRD) study

Crystalline materials exhibit characteristic peaks in an XRD graph. The nature of lyophilized KOF1 and blank SLNs was thus assessed using XRD (XPERT-PRO, PAN analytical, Netherlands) and compared with pristine KTZ. The test sample was exposed to CuKα radiation (45 kV, 40 mA) with scanning angle ranging between 5 and 50°. The values of 2θ and scanning step time were 0.017° and 25s, respectively.

Surface morphology analysis

Surface morphology of prepared KTZ-SLNs (KOF1) was examined by high-resolution transmission electron microscopy (HR-TEM) and field emission scanning electron microscopy (FE-SEM). Prior to observation under HR-TEM and FE-SEM, KOF1 were diluted (50 X) with distilled water. The procedure for FE-SEM included placing the KTZ-SLN dispersion on Nucleopore Track-Etch membrane and drying at room temperature. Dried membrane was attached to the silicon wafer using double-sided carbon tape followed by sputter coating with gold and observing under FE-SEM (FE-SEM SU8000, Hitachi, Japan). For HR-TEM, KTZ-SLNs were stained with 0.2% w/v of phosphotungstic acid in phosphate buffer at pH 6.8, for 5 min. Then, the excess phosphotungstic acid was removed using filter paper. The stained sample was spread over carbon-coated copper grid and was observed under HR-TEM (H-7500, Hitachi, Japan) at a voltage of 200 kV, for morphology (shape and size).

HPLC method

KTZ was quantified using a validated HPLC (high-performance liquid chromatography) method suitably modified from the reported method [25]. A standard plot and the drug analysis were carried out using HPLC Waters, Empower 2, software (USA) equipped with a reverse phase C_{18} column (150 mm × 46 mm, 5μ particle size) at ambient temperature (operational temperature, 25 ± 1 °C). The drug was eluted using a mobile phase composed of acetonitrile, and phosphate buffer pH 4.5 in the ratio of 48:52 (v/v). The mobile phase was freshly prepared, filtered (using a membrane filter), and bath-sonicated to avoid entrapped air and suspended particles (if present). The sample (20 µL) was injected and analysed at a flow rate of 1 mL/min over total run time of 10 min. The drug was assayed at 230 nm using a PDA detector and the column temperature was maintained at 45 °C. A stock solution of KTZ was prepared in methanol and then a standard concentration range (0.2–20 µg/mL) was prepared to construct a calibration plot between concentrations versus area under the curves at a regression coefficient (r^2) of 0.999. The analysis was replicated to get mean and standard deviation ($n = 3$).

Release behaviour and mechanism

In vitro release pattern of KOF1 was studied using a dialysis membrane (12 K Dalton molecular weight cut-offs, HiMedia, Laboratories, Pvt., Mumbai, India) as per reported method [26, 27]. A fixed volume (1 mL) of KOF1 and KTZ-SUS containing 20 mg of KTZ was loaded in the dialysis membrane (HiMedia, Laboratories, Pvt., Mumbai, India; molecular weight cut-off of 12 KDa; semi permeable membrane). The dialysis membrane was soaked in water for 12h before experiment. The dialysis membrane containing sample was suspended in a release medium (phosphate buffer solution, pH 7.4). Sink condition was maintained using dimethyl sulfoxide (DMSO; 5% v/v). Sampling (2 mL) was carried out at various time points (1, 2, 4, 8, 12, 16, 24, 48, and 72h). The withdrawn volume was replaced with fresh release medium (equal volume) at each time point. The withdrawn sample was filtered and analysed using the validated HPLC method at λ_{max} of 230 nm. Analysis was replicated for mean and standard deviation ($n = 6$). Finally, various mathematical models were applied to investigate release mechanism (zero-order, first-order release, Higuchi model and Korsmeyer-Peppas model).

Ex vivo performance across rat skin

Drug permeation studies

Permeation potential and drug deposition were carried out using Franz diffusion cells as per reported method [28]. KOF1 was compared against KTZ-SUS and marketed product (Nizral® 2% w/v; Jenssen Pharmaceuticals). For this, rat skin (abdominal) was freed of hair using a digit trimmer without making any surgical cuts or injury. The excised and trimmed skin was placed between two chambers of Franz diffusion cell such that the outer stratum corneum side faces the donor compartment on which the formulation is mounted and the inner dermal skin layer is towards the receptor medium (PBS, pH 7.4). The receptor chamber was filled with release medium (30 mL) and set at 32 ± 1 °C under constant stirring using a Teflon-coated magnetic bead [29]. The test sample (0.5 mL containing10 mg KTZ) was placed over exposed skin (available surface area of 2.1 cm^2). Three treatment samples (KOF1, KTZ-SUS, and KTZ-MKT) were studied separately under similar experimental conditions. The donor chamber was properly covered with paraffin film to avoid loss of solvent or dryness of the sample. The sampling was performed at different time points (0.3, 1, 2, 4, 6, 8, 12, 24, 48, and 72h) followed by

replacing equivalent volume of withdrawn sample with fresh release medium. Notably, DMSO (5% w/v) was added to the receptor medium to maintain sink condition. The withdrawn sample was filtered using a membrane filter (0.2 µm). The permeated amount of the drug across the skin was estimated using HPLC. Several permeation parameters (cumulative amount of drug permeation, permeation flux, and enhancement ratio) were calculated [30]. After completion of permeation study, the skin samples were removed and washed with running water for drug deposition (retention) study. The experiment was replicated for mean and standard deviation values ($n = 6$).

Skin retention studies

This study is an extension of the skin permeation study. After completion of the permeation study, the skin was washed with running water to remove adhering treatment sample. Then, the skin was sliced into small pieces using a surgical scissor and placed in a solution containing methanol and chloroform (2:1 ratio) [31]. The drug deposited or retained in the skin was extracted over 12h under constant stirring at room temperature. The sample was filtered and centrifuged (9000 rpm) for 15 min to get the clear supernatant. The obtained supernatant was analysed for the amount of the drug retained in the skin, using HPLC. The study was repeated for mean and standard values ($n = 6$).

Bioanalytical method

A 10% homogenate of rat skin was prepared in cold 150 mM KCl solution and centrifuged at 9000 rpm for 10 min. To 300 µl skin supernatant samples in an Eppendorf tube, 700 µl of chloroform:methanol (2:1) was added. The sample was vortexed for 8 min and centrifuged at 15,000 rpm for 10 min to remove precipitated proteins. The supernatant was transferred to a labelled tube, evaporated to dryness, and reconstituted with 400 µl mobile phase comprising acetonitrile and 25 mM phosphate buffer pH 4.5 in the ratio of 48:52 (v/v). Resulting solution was filtered through a 0.2-µm syringe filter and injected in HPLC for analysis. Skin samples were prepared by spiking with 100 µL each of the appropriate working dilution of KTZ to result in concentrations lying within 0.2 to 20 µg/mL. The recovery of KTZ from skin samples was 70–76%.The analysis was replicated to get mean and standard deviation ($n = 3$).

Dermatokinetics: an in vivo study

The animal study was carried out in Wistar albino rats weighing about 250–300 g of both sexes. They were issued from Institutional Animal House UIPS (University Institute of Pharmaceutical Sciences) (Approved as regd. No.45/GO/ReBiBt/S/99/CPCSEA). All of the animals were housed in a conditioned room with free access of food and water as per guideline. Animals were randomly selected and grouped ($n = 6$ per group) as per treatment schedule. The body surface of rats was properly inspected for any possible injury and abnormality. The dorsal surface was used to locate a site of application by making three areas (3 cm^2) free of hairs. Each group received all three formulations at labelled location on the dorsal site. After 24h of shaving, formulations (KTZ-SLNs, KTZ-SUS, and KTZ-MKT) were applied with equivalent concentration and dose strength. Rat was ethically sacrificed at varied time points (2, 6, 12, 24, 48, and 72h) for dermatokinetic study. Three skin samples were excised from the applied site and washed with water to remove adhered content. Then, the skin samples were sliced into small pieces to extract the drug content by dispersing in a mixture of chloroform and methanol (2:1). The mixture was homogenized after 8 h and filtered. The filtrate was centrifuged to get a supernatant. The supernatant was used to estimate the extracted amount of the drug by HPLC method. The data obtained was fitted into one compartment open model. For dermatokinetics profile, the drug concentration versus time profile is presented as a graph using a PK solver (version 1.1). Several dermatokinetics parameters such as area under the curve (AUC0–72 and $AUC_{0-\infty}$), the maximum drug concentration reached in the skin layer (C_{max}), and the time required to attain C_{max} as T_{max} were assessed. The experiment was replicated for mean and standard deviation values ($n = 6$).

Fluorescence microscopy study

This was conducted to visualize the tailored SLNs labelled with a fluorescent probe, using dermatome human skin. Approximately 30 µL of 2% aqueous solution of fluorescein taken as control or corresponding FL-SLNs was applied topically to the surface of skin. At 2h and 24h after treatment, skin sections were cut and fixed. Fluorescein was excited at 470 nm and the fluorescent emission was detected at 515 nm. Several representative images of the treated skin were visualized using fluorescent microscopy (IX71 Olympus Inverted Microscope, Olympus, Tokyo, Japan) with a 10× magnification.

Vibrational spectroscopic imaging techniques in human skin

Skin treatment procedure

Flash-frozen human skin with thickness 4cm^2 (T-SKN-FF2CM) purchased from a licensed supplier (ZenBioInc, USA) was used for this study. All of the skin samples used

in this study were from the same donor. 2.5 cm × 2.5 cm piece of skin was cut and cleaned. Formulations (KTZ-SLNs and KTZ-SUS) were applied topically on the skin surface in excess. Product was massaged on the skin using a glass rod and allowed to sit for 5 min. Skin was placed on a Franz diffusion cell for 3 and 24h at 32 °C. After 3 and 24h, the excess product on the skin surface was gently blotted with a wet Kimwipe. To evaluate product penetration inside the skin, sample preparations were used. Transverse skin sections (8 µm) were obtained using cryo-microtome and scanned by ATR-FTIR imaging to visualize product penetration inside the different skin layers. Skin cross-sections (8 µm) were cut using a cryostat. These cross-sections were scanned by ATR-FTIR imaging to evaluate product penetration inside the epidermis. ATR-FTIR images of the cross-sections were recorded with a Spotlight 400 System (PerkinElmer Instruments, Shelton, CT, USA), consisting of a FTIR spectrometer with a mercury-cadmium-telluride (MCT) focal plane array detector. Images were collected in reflective mode at a spectral resolution of 4 cm^{-1} and 4 scans accumulations in the mid-infrared (MIR) region between 4000 and 750 cm^{-1} with a spatial resolution of 6.25 × 6.25 µm at room temperature (24 °C). The ATR imaging accessory used a germanium crystal placed directly in contact with the skin samples. All the data were processed (baseline correction, generation of spectroscopic parameters) using GRAMS/AI (Thermo Fisher Scientific) or ISys software from Spectral Dimensions (Olney, MD).

Confocal Raman spectroscopy imaging

Skin was also scanned by confocal Raman spectroscopy to evaluate product penetration inside the stratum corneum and beyond in the epidermis. Human skin was treated for 24h at 34 °C. After incubation, skin was placed in a home-built brass cell. Confocal Raman images were acquired with a WITec Alpha-3000R plus confocal Raman microscope (Ulm, Germany) equipped with a 532-nm laser. XZ images were taken for each sample. The XZ depth image was typically 50 × 30µm^2 covering SC and upper viable epidermis (VE) region with 4-µm steps and a 20-s exposure time.

Stability studies

Photostability

It was conducted for KTZ-SLNs and KTZ-SUS as per ICH guidelines Q1B [32]. The freshly prepared samples were packed in amber-coloured and clear glass vials, labelled, and recorded for further process. Each batch was exposed to illumination light of 1.2 million lux h and an integrated near UV energy (200 W h/m^2) for 10 days in a photostability chamber (Binder Gmbh, Germany). All experiments were repeated for mean and standard deviations ($n = 6$).

Long and accelerated stability

A long-term accelerated stability of the developed formulations (KTZ-SLNs) was conducted as per ICH Q1A guidelines [33]. A constant amount of each formulation was transferred to fresh and clean amber-coloured glass container. Three batches for each formulations were prepared, packed, and labelled as per experimental schedule 4 °C (2–8 °C), 30 (± 2 °C)/65% (± 5%) RH and 40 (± 2 °C)/75% (± 5%) RH). The samples were withdrawn at 0, 30, 90, 180, and 360 days, and evaluated for particle size, %EE, and the drug assay/content (%). All experiments were repeated for mean and standard deviations ($n = 6$).

Results and discussion

Preparation of formulation and pre-optimization

Initially, several trial formulations were prepared using the investigated lipid (CATO as lipid), surfactant (tween 80), co-surfactant (PEG600), and stabilizer (P90G) as per Taguchi design (Table 1). Moreover, the design was used to select factors and levels (Table 1). Several trial formulations were prepared by varying run cycles, speed, and time for homogenization using HPH as shown in Table 1.

The formulation exhibiting overnight benchtop stability was selected for identifying lower and higher levels of each factor for Design Expert (central composite design) (Table 2).We selected X_1 (CATO as lipid) and X_2 (tween 80) as independent factors at three levels as shown in Table 2. The set responses were Y_1, Y_2, and Y_3 for particle size (nm), %EE, and the drug content (%), respectively. This tool is reliable to obtain the most robust formulation with optimum content of the solid lipid and surfactant under set desired goals. Moreover, the software was used to identify the potential factors affecting dependent variables (Y_1–Y_3) and possible interaction between factors (X_1 and X_2). The central composite design (CCD) suggested thirteen formulations under given set of constraints and goal. The suitability of the model was assessed by analysis of variance (ANOVA). The statistical parameters (p, F, and r^2 values) were carefully examined for the model to be fit. All responses (Y_1–Y_3) followed quadratic model and the generated polynomial equations are presented in Table 2. The negative and positive signs associated with each term represent antagonistic and synergistic influence of individual factor on the investigated responses, respectively.

Particle size (Y_1) of SLNs dispersion is a significant parameter for efficient in vitro and in vivo experiments. The

Table 1 Taguchi design variables

		–1	(+1)	
	Code factor	**Levels**		**Response**
A	Lipid (%)	8.0	10.0	Particle size (nm)
B	Tween 80 (%)	3.0	7.0	Entrapment efficiency (%)
C	PEG600 (%)	2.0	6.0	
D	Phospholipon 90 G (%)	0.1	0.3	
E	Stirring speed (rpm)	8000	10000	
F	Stirring time (min)	8	10	
G	Homogenization Cycle	5	7	

Std	**Run**	**A**	**B**	**C**	**D**	**E**	**F**	**G**
5	1	8.0	3.0	6.0	0.3	8000	8	5
1	2	8.0	3.0	2.0	0.3	10000	10	7
7	3	8.0	7.0	2.0	0.1	8000	10	5
4	4	10.0	7.0	2.0	0.3	8000	8	5
3	5	8.0	7.0	2.0	0.1	10000	8	7
6	6	10.0	3.0	6.0	0.1	10000	8	5
8	7	10.0	7.0	6.0	0.3	10000	10	7
2	8	10.0	3.0	2.0	0.1	8000	10	7

nanoscaled safeguard circumvents direct interaction of KTZ with efflux proteins thus ensuring its entry into the fungal cells. Furthermore, lower particle size reduces the tendency of coalescence which leads to increase in stability and shelf life of KTZ-SLN formulation. The polynomial equation for Y_1 is given in Table 2 where negative signs of coefficients associated with both factors X_1 and X_2 indicate that these factors need to be reduced to get desired response. The 3- and 2-dimensional contour plots for Y_1–Y_3 are illustrated in Fig. 1. The result showed that Y_1 increases with increase in X_1 (CATO) which may be due to higher content of lipid (Fig. 1A and B). Therefore, it should be reduced to an optimal level. In contrast, Y_1 was at first found to decrease with decrease in tween 80 content while it increased on further reduction in X_2. Thus, both X_1 and X_2 need to be optimized to get the most robust SLNs. The lower value of p (0.0006) and high F (21.97) value confirmed the best fit of the model adopted for analysis of Y_1. Moreover, the adjusted correlation coefficient (r^2) was close to the observed value which suggested good fit of the model. The optimum particle size (minimum) was due to relatively higher concentration of surfactant (7% w/v) and optimal lipid content 10% w/v. However, with further increase in concentrations of both the factors, there was increase in particle size due to micelle formation. Hence, it may be concluded that to obtain optimized formulation, the optimum levels of X_1 and X_2 are required. For Y_2, the positive signs of X_1 and X_2 associated with first and second terms of the quadratic equation (Table 2) suggested that the concentrations of X_1 and X_2 should be at high level for the optimized product. Thus, the effect of the concentration of lipid and tween 80 is directly proportional to Y_2. These two were found to be considerable factors to use in optimal concentration. The result is exhibited in Fig. 1C and D (response surface and 2-D contour plots) where Y_2 was found to increase linearly on increasing the content of X_1 which may be due to increased solubility of lipophilic KTZ in lipid. Compritol®888 ATO is a complex lipid composed of mixtures of mono-, di-, and triglycerides which form less perfect crystals, and accord space to accommodate drug molecules [34].

Furthermore, Y_2 was found to increase with increasing content of tween 80 (X_2). Statistical analysis suggested that the model was the best fit for this response as evidenced with high value of F (19.68), low p value (0.0008), and the closeness of r^2 between adjusted (0.9842) and predicted ($r^2 = 0.9766$) values. The generated quadratic equation is presented in Table 2 with associated coefficients in each term. The total drug content is a significant parameter for assessing stability and shelf life of the formulation. It was expected that the drug content (Y_3) should increase with increase in X_1 and X_2 due to drug solubility in lipid- and surfactant-based improved emulsification. The drug content was the highest when both the factors (X_1 and X_2) were at axial point (X_1: + 1 and X_2: + 1) (Fig. 1E and F). The mathematical relationship of Y_3 to factors is represented by the quadratic equation obtained and presented in Table 2. When the lipid and tween 80 concentrations were at optimum point ($X_1 = 10\%$ w/v g and $X_2 = 7\%$ w/v), total drug content of KTZ loaded in SLNs (KTZ-SLN4) as in Table 2 showed maximal value of 96.2%. The model was significant ($p = 0.0009$) and fit as evidenced with the correlation coefficient (regular $r^2 = 0.9878$) and adjusted r^2 (0.9791).

Table 2 Optimization (central composite design)

Level of factors						
Code and factors	$-\alpha$	−1	0	+1		$+\alpha$
X_1:CATO (%)	8	9	9.5	10		12
X_2:Tween 80(%)	3%	4	6	7		8
Constraints						
Code and responses	**Low**		**High**		**Goal**	
Y_1: Particle size (nm)	291.5		843.2		Minimum	
Y_2: EE (%)	35.5		84.6		Maximum	
Y_3: Total drug (%)	77.9		96.2		Maximum	
Formulation code	X_1	X_2	Y_1	Y_2		Y_3
KTZ–SLN1	+1	+1	391.5 ± 12.5	60.7 ± 0.42		78.6 ± 1.4
KTZ–SLN2	−1	−1	780.8 ± 13.2	35.5 ± 0.61		75.5 ± 1.7
KTZ–SLN3	0	0	453.6 ± 9.1	66.7 ± 0.57		80.1 ± 0.9
KTZ–SLN4	−1	+1	291.5 ± 6.3	84.6 ± 0.32		96.2 ± 1.3
KTZ–SLN5	0	$-\alpha$	843.2 ± 17.2	42.6 ± 0.49		83.4 ± 1.5
KTZ–SLN6	0	0	450.4 ± 13.7	62.4 ± 0.51		85.6 ± 0.8
KTZ–SLN7	+1	−1	821.5 ± 19.6	67.4 ± 0.31		88.7 ± 1.4
KTZ–SLN8	$+\alpha$	0	492.6 ± 8.2	66.3 ± 0.51		81.5 ± 1.7
KTZ–SLN9	0	0	449.8 ± 9.3	62.6 ± 0.38		80.1 ± 1.5
KTZ–SLN10	0	$+\alpha$	424.8 ± 11.5	76.7 ± 0.41		82.3 ± 1.1
KTZ–SLN11	0	0	457.4 ± 7.9	62.5 ± 0.61		84.4 ± 0.9
KTZ–SLN12	0	0	455.2 ± 10.2	64.3 ± 0.55		85.6 ± 1.2
KTZ–SLN13	$-\alpha$	0	635.2 ± 7.5	45.60 ± 0.4		79.4 ± 0.7
Composition and statistical analysis of KOF1						
KOF1 as optimized formulation						
X_1: 10% (w/v)						
X_2: 7% (w/v)						
Response	**Model**	r^2	**Adjusted** r^2	***f* value**		***p* value**
Particle size (Y_1)	Quadratic	0.991	0.982	21.97		0.0006
%EE (Y_2)	Quadratic	0.9766	0.9842	19.68		0.0008
Total drug (Y_3)	Quadratic	0.9878	0.9791	8.80		0.0009

Table 2 (continued)

Level of factors			
Generated polynomial equations			
$Y_1 = 2615.98 - 354.27X_1 - 416.84X_2 - 17.16X_1X_2 + 32.34X_1^2 + 52.26X_2^2$			
$Y_2 = -173.36 + 51.95X_1 + 14.64X_2 - 1.42X_1X_2 - 2.85X_1^2 + 0.43X_2^2$			
$Y_3 = 134.38 - 19.35X_1 - 7.91X_2 - 1.23X_1X_2 + 1.78X_1^2 + 0.19X_2^2$			
Optimized KOF1	Y_1 (nm)	Y_2 (%)	Y_3 (%)
Observed value	293	88.5	96.25
Predicted value	289	84.0	95.00
% Bias	1.36	5.08	1.30

Optimization and validation parameter

Based on statistical parameters for the responses Y_1–Y_3, the most robust formulation was obtained with optimum content of X_1 and higher content of X_2 to achieve the set goal. The predicted and observed values were closely related as evidenced with correlation coefficient value ($R^2 > 0.90$) all explored responses (Y_1–Y_3) (Fig. 2A-C). There were no observed interaction for Y_1 and Y_2 (Fig. 2D and E). However, the response Y_3 exhibited a slight interaction between factors (Fig. 2F). The value of overall desirability function was obtained as 0.907 close to unity. Thus, the used model was the best fit under given set of experimental conditions and importance to each factor and response. The most optimized formulation obtained was KOF1 with the highest desirability function parameter as compared to other suggested formulations (Fig. 3).

Post-optimization studies: evaluation parameters of KTZ-SLNs (KOF1)

Particle size, PDI, zeta potential, EE, and drug assay/TDC

The finally optimized formulation KOF1 was comprised of X_1 (10% w/v) and X_2 (7% w/v) with maximum desirability value. The results of particle size (Y_1), PDI, and zeta potential were found as 293 ± 6 nm, 0.258 ± 0.07, and -22.92 ± 2.4 mV, respectively, for KOF1 (Table 2). Moreover, the results of %EE (Y_2) and % drug assay/total drug content (Y_3) were found to be as $88.5 \pm 1.5\%$ and $96.25 \pm 0.85\%$ for KOF1, respectively. Notably, the concentration of KTZ in final formulation of SLNs was 0.2% w/v in our previous report published for ocular delivery [20]. The present study was intended for topical delivery of KTZ to control fungal infections caused by the resistant and sensitive strains residing into the deeper epidermal tissue. Therefore, higher strength (2% w/v) was formulated and evaluated for in vitro, ex vivo, and in vivo performance as compared to marketed and prepared suspension. The predicted values of particle size, %EE, and % drug content were 289.0 nm, 84%, and 95%, respectively, for KOF1 suggesting good agreement of the model fit due to closeness of the predicted values to the observed values. In the case of dye-loaded SLNs (FL-SLNs), the particle size was 298 ± 2 nm and PDI was 0.218 ± 0.03. Furthermore, lyophilized powder of KTZ-SLNs was reconstituted with 10 mL of water and evaluated for particle size analysis. Obtained particle size was 307 ± 3 nm and PDI was 0.267 ± 0.06. Thus, there was not much change in particle size and size distribution when probed with the dye and on reconstitution after lyophilization.

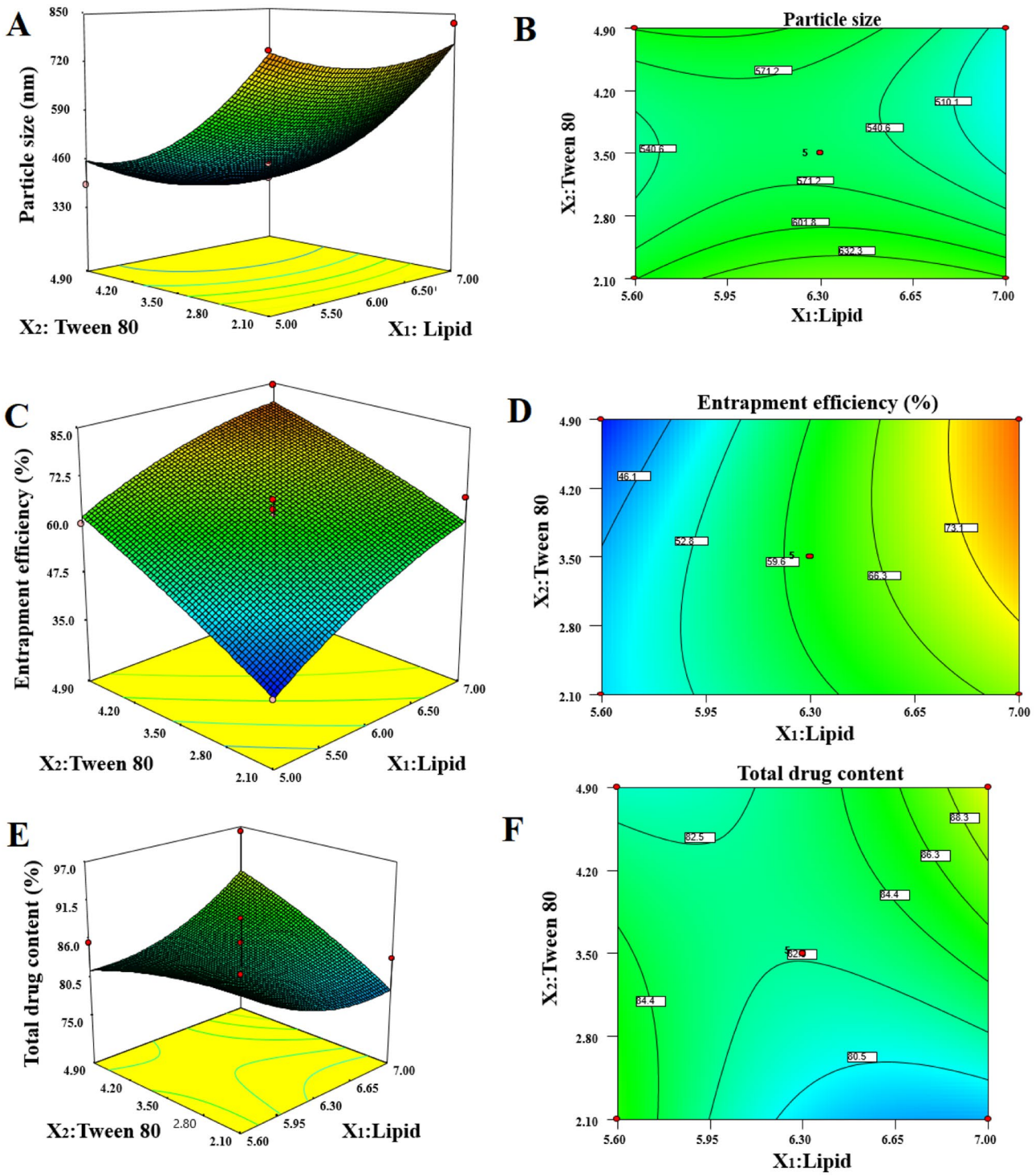

Fig. 1 Three-dimensional response surface and 2-dimensionl contour plots showing the influence of Compritol ATO 888 (lipid) and tween 80 (surfactant) on particle size (Y_1) (**A**–**B**), %EE (Y_2) (**C**–**D**), and % total drug content (Y_3) (**E**–**F**)

Differential scanning calorimetry (DSC)

Melting (heating) of lipid and recrystallization (cooling) of hot lipidic emulsion after passing through HPH to form solid lipid nanoparticles may change the crystalline behaviour as well as the polymorphic form of the lipid. As illustrated in Fig. 4A and B, the characteristic sharp endothermic peaks were obtained for lipid and the drug at

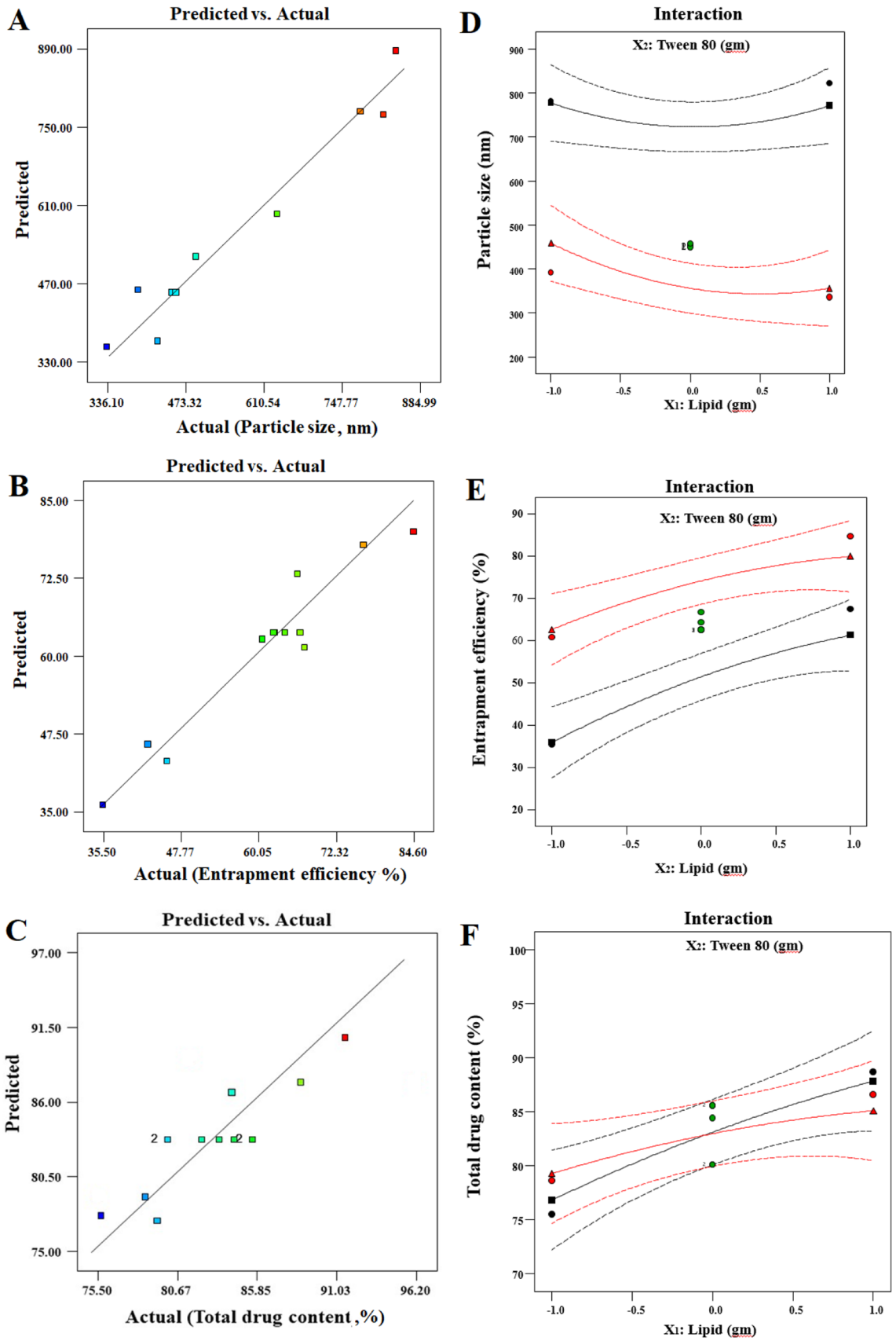

Fig. 2 Predicted and observed values of responses Y_1–Y_3 (**A**–**C**) and interaction curves (**D**–**F**)

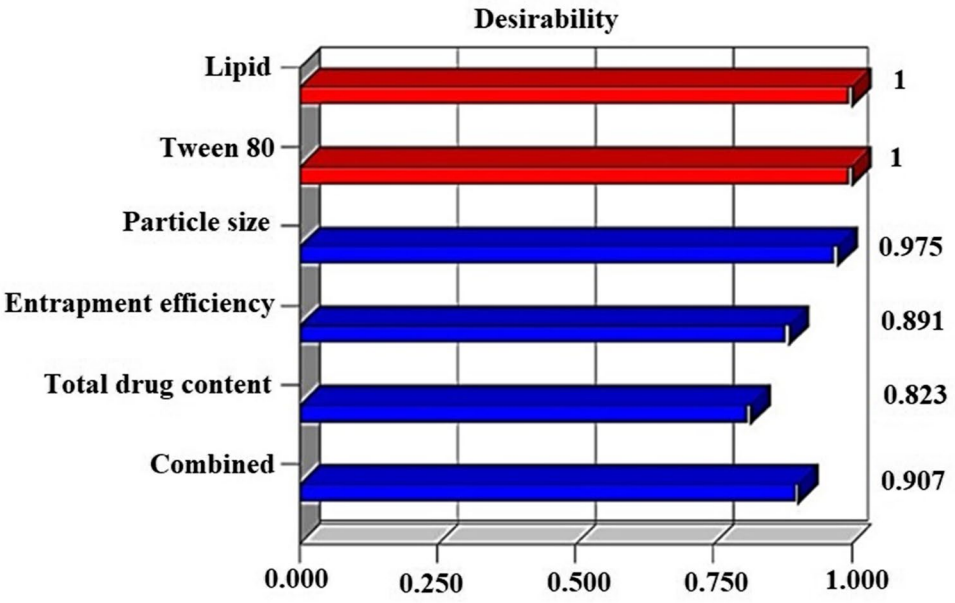

Fig. 3 Desirability function parameter for the optimized KTZ-SLNs (KOF1)

75.6 °C (486.9 J/g) and 153.7 °C (269.5 J/g), respectively. In literature, the melting points of the Compritol 888 ATO (lipid) and KTZ are indicated as 71.7 °C and 151.22 °C, respectively, and are in close agreement with the presently obtained values [35]. DSC for KTZ does not exhibit any degradation endothermic peak at or around 75 °C, which was the temperature at which SLNs were prepared, thus confirming that ketoconazole was stable during SLN preparation. Chemically, the used solid lipid is glycerol esters of behenic acid (C_{22}) containing behenic acid as major constituent (>85%). Moreover, the lipid is amphiphilic (HLB ~ 2) in nature due to the presence of partial acylglycerol. It is noteworthy that the lipid has low peroxide value (6 meq O_2 Kg^{-1}) suggesting high chemical stability [35]. Therefore, this lipid was selected to load chemically challenged KTZ for improved solubility and chemical stability. KTZ-SLNs (KOF1) however showed broad and multiple endothermic peaks that shift to 89.39 °C and a significantly lowered heat flow of 92.26 J/g, which indicates the incorporation of KTZ into the lipid matrix (Fig. 4C). Lower enthalpy value for KTZ-SLNs (KOF1) with respect to both the free KTZ and the lipid indicates solubilized KTZ in the lipid matrix having more imperfections in the crystal lattice which can accommodate more drug content in their crystal lattice [36]. Both blank and KTZ-SLNs (KOF1) showed multiple peaks (Fig. 4C and D). DSC of polyethylene glycol 600 (PEG 600) and Phospholipon 90 G (P 90G) also indicate several endothermic peaks (Fig. 4E and F). Peaks corresponding to Compritol 888 ATO (CATO) exhibited at 74.65 °C (486.9 J/g) (Fig. 4B) shifted to 78.59 °C in KOF1, but it was associated with a lower enthalpy of 370.2 J/g indicating shift towards amorphousness. This is expected of the SLN lipid matrix incorporating KTZ and also PEG 600 [20]. Partial shift of peak corresponding to CATO to higher temperature could be due to merging with the shoulder exhibited by PEG 600 at 78.43 °C, considering that the latter is present at a significant concentration of 6% w/v in KTZ-SLNs. KTZ-SLNs did not exhibit any peak corresponding to 153.73 °C as exhibited by pure KTZ. However, there was a peak at 104.52 °C which is partly attributed to a shoulder exhibited at 117.74 °C by P 90 G and a peak exhibited by PEG 600 at 95.28 °C. Both PEG 600 and P 90G form a layer around the lipid matrix of SLNs [20] as also indicated in HR-TEM of KTZ-SLNs [17]. Similarly peak is also observable at 111.04 °C for blank SLNs (Fig. 4D) and is associated with a high enthalpy of 2370 J/g versus 942.8 J/g for KTZ-SLNs. Presence of KTZ in the outer surfactant (PEG 600 and P 90G) layer of KTZ-SLNs as described previously [17] may attribute to the lower enthalpy. The same is apparent from the release data (Fig. 7A).

Fourier transform infrared spectroscopy (FTIR)

The result of FTIR study is portrayed in Fig. 5A wherein pure KTZ, KOF1, and blank SLNs exhibited characteristic peaks. Notably, pure KTZ showed prominent stretching peaks at 1510 cm^{-1} for unsaturated hydrocarbon (C = C), 1646 cm^{-1} for carbonyl group, 1036 cm^{-1} for aliphatic ether, 1245 cm^{-1} for cyclic ether, and 817 cm^{-1} for halogen attached with carbon (C–Cl). These values were in agreement with reported stretching [37]. A major peak

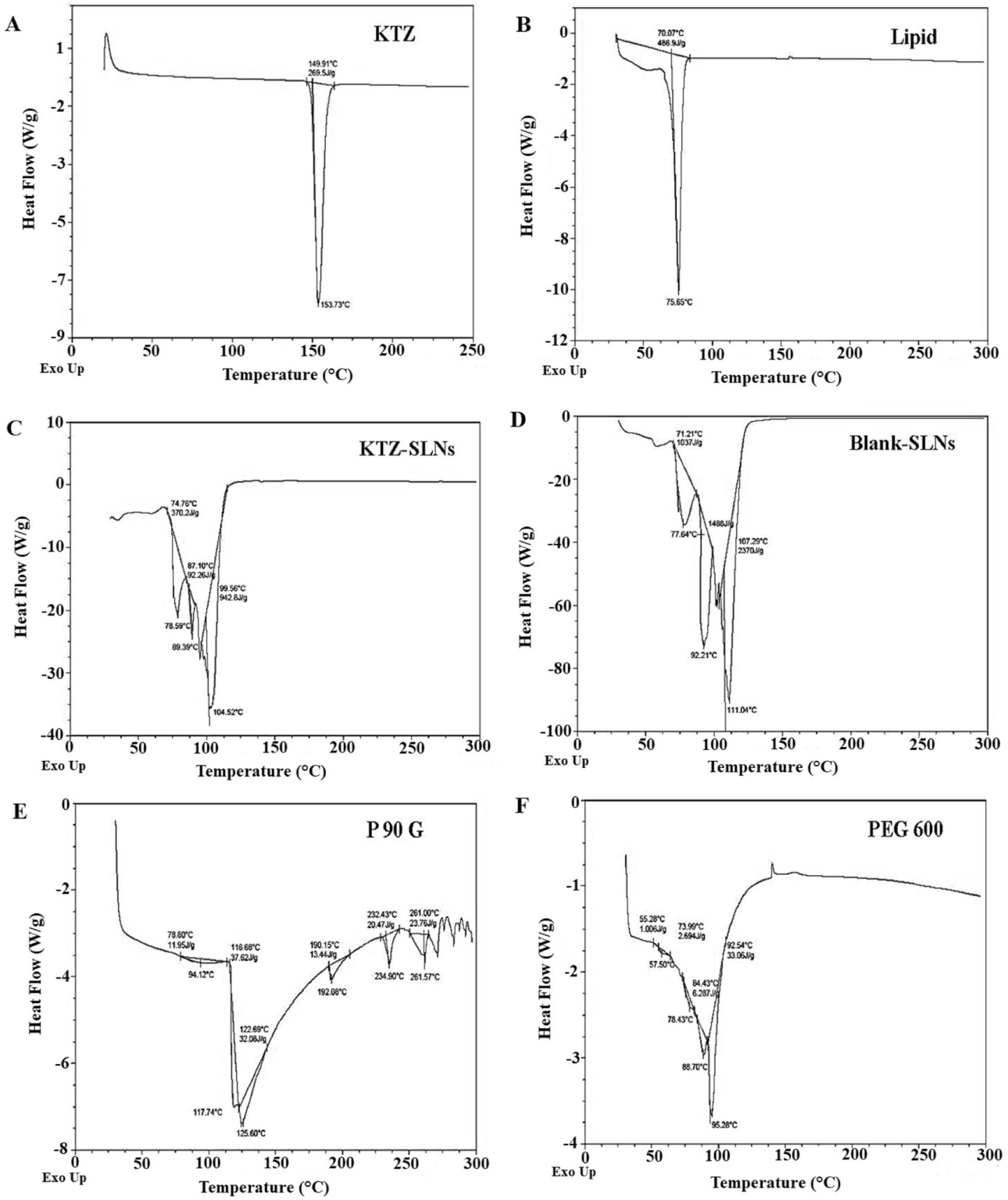

Fig. 4 DSC thermograms of (**A**) pure KTZ, (**B**) pure lipid, (**C**) KTZ-SLNs, (**D**) blank SLNs, (**E**) P90 G, and (**F**) PEG600

retained at 2923 cm^{-1} and 2047 cm^{-1} in blank SLNs and KOF1 is due to stretching vibration of C-H group present in lipid excipient. Moreover, remarkable band from 1711 to 1742 cm^{-1} corresponds to carbonyl group (C = O) and from 1578 to 1609 cm^{-1} corresponding to unsaturated carbon (C = C) is associated with the lipid excipients

of formulation [38]. In KOF1, few characteristic peaks of the drug (2962–2836 cm^{-1} assigned for C-H stretching, 1652 cm^{-1} for C = O stretching vibration), lipid (14,898–1553 cm^{-1}), and other excipients were retained with slight variation in intensities. Few peaks of the drug (for C-N and C–Cl) overlapped with the lipid [39].

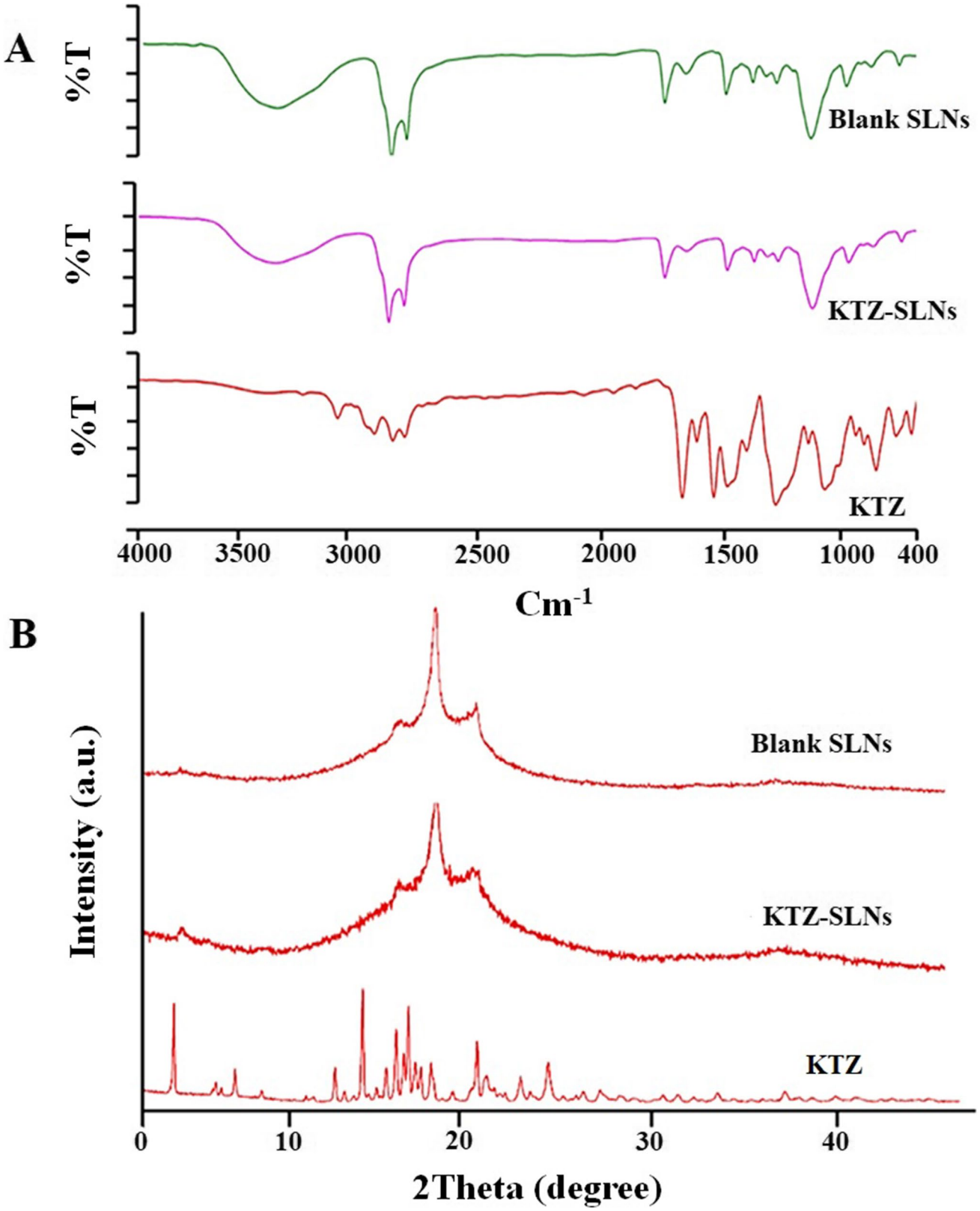

Fig. 5 Evaluation of KOF1, blank formulation, and pure KTZ: (**A**) FTIR spectra and (**B**) powder X-ray diffraction study

Powder X-ray diffraction (PXRD)

This was carried out to identify the solid-state characteristic behaviour of the pure KTZ and developed formulation. The technique was helpful to identify crystallinity and amorphous nature of the drug and KTZ-SLNs, respectively, as shown in Fig. 5B. The lyophilized KTZ-SLNs and blank formulation were found to be amorphous as compared to pure KTZ. This confirmed that the KTZ-loaded SLN formulation was relatively soluble as compared to pure drug. KTZ exhibited remarkable peaks with 2θ values of 7.2, 17.4, 19.8, 22.2, and 24.9. These suggested the crystalline nature of the drug and were found to be complying with a previous report [40]. Blank formulation revealed an amorphous nature due to blend of lipid with surfactant and stabilizer. The lack of characteristic peaks of the drug in KOF1 may be due to solubilized form of KTZ amalgamated completely in lipid matrix or molecularly dispersed or amorphous state of KTZ [21]. Moreover, this suggested the least unentrapped drug outside the lipid core.

Surface morphology analysis

FE-SEM and HR-TEM are two advanced and sophisticated technologies to visualize morphological behaviour of nanomedicine or nanocarrier at varied resolution and magnification. The shape and size of the particle are important aspects to assess in vivo performance of nanomedicine. The representative images of FE-SEM and HR-TEM are presented in Fig. 6A and B. The high magnification (10,000×) HR-TEM image illustrated that the lipid core was enclosed with a hydrophilic firm layer of the surfactant. Acquisition of perfectly spherical shape was attributed to the mixture of surfactant-mediated effective covering around the SLNs surface during homogenization. The size of SLNs observed by HR-TEM was relatively lower than the value obtained in DLS. This variation is associated with several factors such as instrumental error of TEM (relative adsorption of smaller size particle by the grid) and the collapsed SLNs after water evaporation during drying process [41]. It is apparently observed that the optimized KTZ-SLNs (KOF1) were homogeneously dispersed, discrete, and spherical. In general, spherical particles are relatively stable and suitable for improved permeation across skin. Moreover, spherical particles are considered to sustain their shape upon storage while disc shaped or discoid particles tend to aggregate which lead to gelation upon storage [42, 43].

In vitro drug release

KTZ is highly crystalline in nature and poorly soluble in water (0.04 mg/mL) or buffer. In vitro release behaviour of the drug suspension and KTZ-SLNs (KOF1) was determined in PBS (pH 7.4) containing 5% v/v DMSO (to maintain sink condition). It is observed that the drug was poorly released (38%) across the dialysis membrane from the drug suspension over a period of 2h and then no release was observed due to poor solubility of the drug. However, the optimized SLN formulation exhibited an initial burst release within 2h due to free drug and subsequent extended release (99.84%) within 72h (Fig. 7A). KTZ release from SLNs was exponential in first 2h followed by sustained release over 72h which may be attributed to solid lipid matrix amalgamated with the drug. However, 13% of the total loaded drug was released within 2h and these values closely correspond to the free/unentrapped drug present in the KTZ-SLN formulation. Free/unentrapped KTZ was not removed from the SLN dispersion. Though KTZ is insoluble in water or aqueous system resulting in limited permeation across stratum corneum, however, in presently developed KTZ-SLNs, the free drug was present in the solubilized form and did not separate or crystallize out of the system. It is contested that this free drug can act as a (i) loading dose for immediate onset of action, and (ii) also contributes to ensure high entrapment. Further it helps to maintain the thermodynamic equilibrium favouring release of KTZ from within SLNs as the free KTZ is absorbed into skin (in this experiment released into dialyzing fluid).

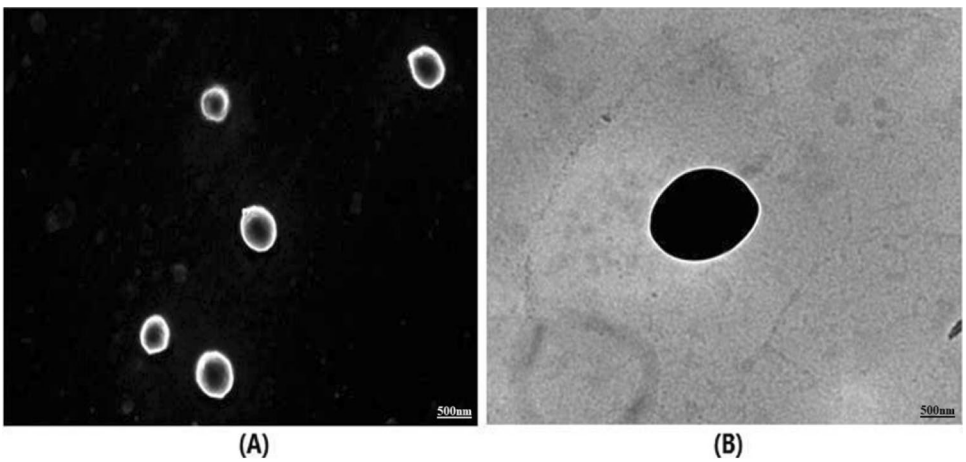

Fig. 6 KTZ-SLNs (KOF1) under FE-SEM at 5000× (**A**) and HR-TEM at 10,000× (**B**)

Different kinetic models were applied to understand the release mechanism of KTZ from the lipid matrix. In the first 12h, KTZ followed non-Fickian release as evidenced from the low "*n*" value (0.82) for the best fit ($r^2 = 0.9948$) Korsmeyer Peppas model. From 24 to 72h, zero-order release model was the best fit model ($r^2 = 0.9961$) for KTZ-SLNs suggesting slow and controlled release from the lipid matrix. This diffusion-controlled release was predicted to occur from porous matrices [44]. The release of drug from a matrix can be predicted based on the various drug release models.

Ex vivo skin permeation and retention studies

The drug permeation profiles of formulations (KTZ-SLNs, KTZ SUS, and KTZ-MKT) are illustrated in Fig. 7B. The cumulative amount of the drug permeated (flux) across rat skin at the end of 72h was 6643.58 ± 210.2 μg/cm^2, 2924.66 ± 90.6 μg/cm^2, and 1134.14 ± 11.3 μg/cm^2 for KTZ-SLNs, KTZ-MKT, and KTZ-SUS, respectively (Fig. 7B; Table 3). Higher permeation of KTZ-SLNs is attributed to the adhesive and occlusive nature of SLNs which improve hydration and thus permeation of the skin [45]. Most studies with such controlled systems are conducted for similar long periods [46] as even though the application may not remain on the skin for this period but the SLNs that permeate will keep releasing the drug over prolonged periods as evidenced from the in vitro data (Fig. 7A). The same can be observed from the retention data at 72h (Fig. 7C). The transdermal flux was the highest at 24h for KTZ-SLN formulation (134.40 ± 4.2 μg/cm^2/h) as compared to KTZ-SUS (23.80 ± 1.8 μg/cm^2/h) and KTZ-MKT (48.31 ± 2.7 μg/cm^2/h), respectively. This improvement is attributed to the structural arrangement of SLN excipients viz. presence of co-surfactant (PEG 600) layer on SLN surface. It being a hydrophilic molecule is incorporated into the polar head group of the skin lipid bilayer resulting in greater penetration via α-keratin and

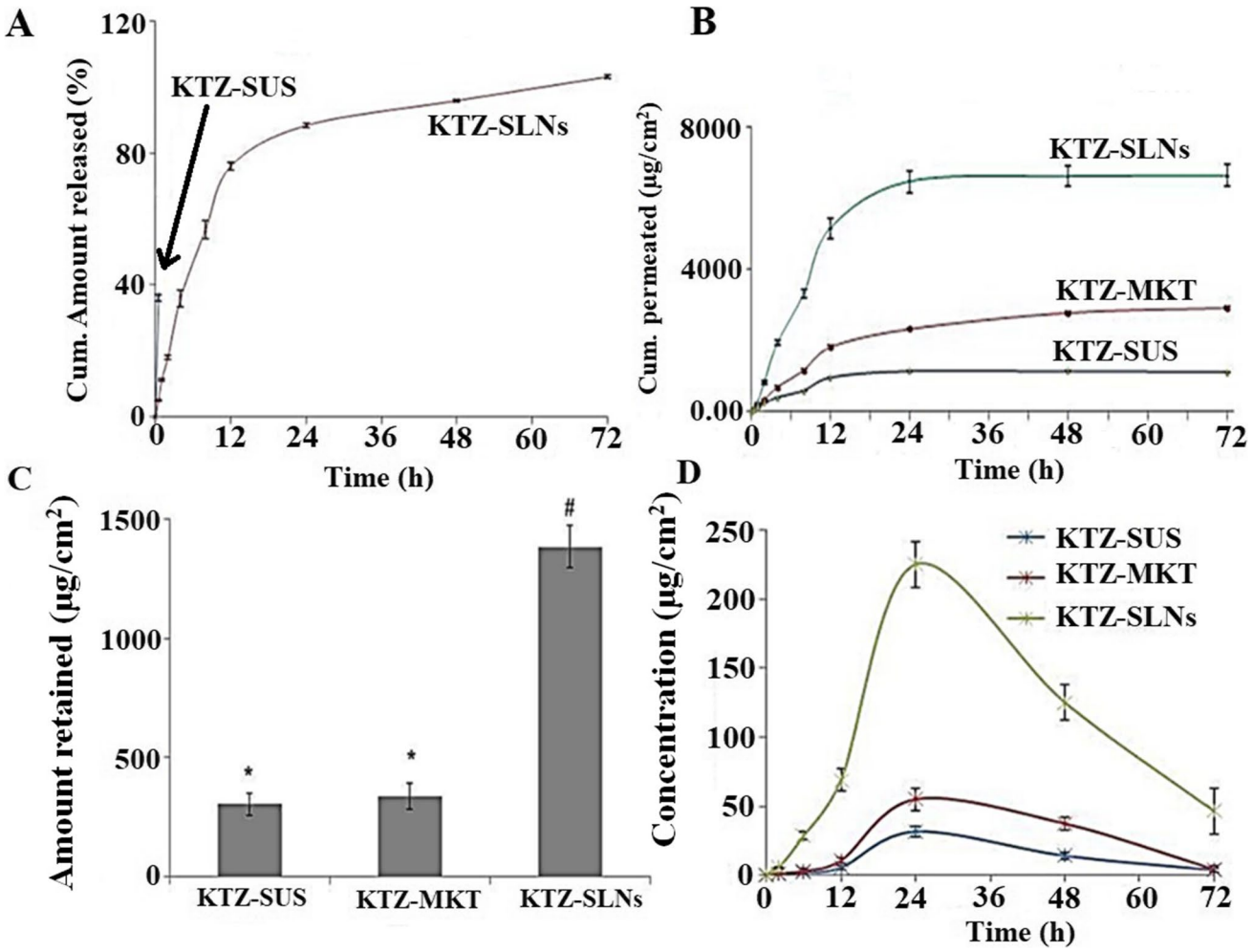

Fig. 7 (**A**) In vitro drug release of KTZ and KTZ-SLNs after 72h ($n = 6$). (**B**) Ex vivo drug permeation study across rat skin illustrating amount of drug permeated from KTZ-SLNs (KOF1), KTZ-SUS, and KTZ-MKT when applied on rat skin placed between a donor and receiver chamber of the Franz diffusion cell ($n = 6$ for each treatment). (**C**) Amount of drug retained per cm^2 into the rat skin after an ex vivo permeation study of KTZ-SLNs (KOF1), KTZ-SUS, and KTZ-MKT ($n = 6$). (**D**) Skin concentration–time profile of KTZ-SLNs (KOF1), KTZ-MKT, and KTZ-SUS following topical application to rat skin ($n = 6$)

other conformational changes in multilamellar lipid bilayer of the SC [43, 44]. SLNs are reported to form a depot in the follicular dermis area [47] from where the encapsulated drug is released due to β to α or β' transition of the lipid [35]. Significant and prolonged KTZ release will thus manage the high fungal load usually found in the deeper skin layers and responsible for relapse [3]. The amount of KTZ present in rat skin at the end of permeation study was also determined (Fig. 7C). As discussed above, it is very important that antifungal drugs reach and stay in deeper layers of skin at optimal concentration, for effective management of fungal infections. The drug retention from KTZ-SLNs was 1383.14 ± 90.3 µg/cm^2 which was 460 and 410% higher than KTZ-SUS (303.81 ± 48.3 µg/cm^2) and KTZ-MKT (336.31 ± 54.4 µg/cm^2), respectively (Fig. 7C). The augmented permeation and drug deposition in the skin is achieved through a combination of physiological and physicochemical mechanisms such as lipid-lipid interaction of skin lipid and SLNs, surfactant-mediated skin lipid extraction for improved permeation, follicular deposition of SLNs for transport to the lower epidermal area, and reduced transepidermal water loss through occlusion achieved on skin surface by SLN application [48, 49].

However, the lower dermal area is highly vascularized and there is a chance of systemic dug transport which is a concern with KTZ due to its hepatotoxic nature. To check if there is any transdermal flux of KTZ applied as KTZ-SLNs, an in vivo study was conducted. KTZ-SLNs were applied on dorsal skin of rats ($n = 3$) after removing hair. The blood was withdrawn from retro-orbital plexus, 72h post application, and was analysed for KTZ, after centrifugation to separate plasma. However, no KTZ was detected in plasma (LLOD: 0.2 µg/mL). This confirms that all KTZ is released and retained in the skin for local action. The flux observed in ex vivo experiments is due to (i) presence of 5% DMSO in receptor media which acts as a penetration enhancer, (ii) large dialysis fluid volume of 30 mL, and (iii) continuous stirring of receptor medium, and all of these factors do not exist in real-time clinical situation.

Dermatokinetic studies

The concentration time profile (Fig. 7D) and dermatokinetic parameters of formulations (KTZ-SLNs, KTZ-SUS, and KTZ-MKT) after topical administration were investigated in rat skin (Table 4). The analytical and bioanalytical method of analysis of KTZ was validated as per USFDA guidelines and showed high accuracy (92.2–96.8%) and precision (1.9–2.9%). Figure 8 shows chromatogram of untreated/blank skin homogenate and following its spiking with KTZ (Fig. 8B), establishing that there was no matrix interference of skin constituents with KTZ peak which was sharp and clear. A recovery of 70–76% was obtained for the spiked skin samples of the standard plot. It was clearly observed that dermatokinetic parameters such as C_{max} (7.1-fold), $AUC_{0-\infty}$ (9.0-fold), and $AUMC_{0-\infty}$ (10.6-fold) were significantly ($p < 0.001$) improved for KTZ-SLNs as compared to KTZ-SUS. Similarly, these parameters for KTZ-SLNs were remarkably increased several times (C_{max} (4.1 times), $AUC_{0-\infty}$ (4.6 times), and $AUMC_{0-\infty}$ (5.6 times)) as compared to commercial KTZ-MKT. Concentration (C_{max}) of KTZ in the skin was significant at 24h (225.19 ± 9.5 µg/mL) and up to 72h (46.32 µg/mL). This indicated prolonged and sustained release of KTZ-SLNs in the skin layers as compared to KTZ-SUS (3.8 µg/mL) and KTZ-MKT (4.4 µg/mL) at 72h. Figure 7D presents skin concentration–time profiles of the KOF1, KTZ-SUS, and KTZ-MKT after topical application on rat skin. It is obvious that KTZ-SLNs improved skin concentration of KTZ when tailored in SLNs as compared to drug suspension and commercial product. The result suggests that the proposed nanoparticles were capable to deliver the drug up to and beyond the viable epidermis which can be suitable for topical fungal infection control. The small particle size of SLN in the nanometre size range causes adherence [28] to the stratum corneum (SC) followed by increased KTZ penetration into viable layer of skin to control fungal cells by lipid-lipid internalization, maximized drug availability around fungal cells, and surfactant-mediated cell wall extraction for detrimental effect [50]. The formed film prevents water evaporation from skin resulting in substantial hydration for augmented penetration of KTZ-SLNs through the stratum corneum [28, 51].

In order to confirm if the topically applied KTZ-SLNs can pass across the skin into systemic circulation, plasma was analysed. No detectable amount of KTZ was present, indicating

Table 3 Comparison of various formulations of ketoconazole in terms of total amount permeated, percentage permeation, steady-state flux (J_{ss}), and apparent permeability coefficient (P_{app}) obtained during ex vivo permeation studies using rat skin (mean ± SD, n = 6)

Formulation	Cumulative drug permeated in 72h (µg)	J_{ss} at 24h (µg/h/cm^2)	J_{ss} 72h (µg/h/cm^2)	P_{app} (cm/s)
KTZ-SUS	1134.01 ± 13.84	23.80 ± 1.8	7.83 ± 1.3	2.82
KTZ-MKT	2924.61 ± 32.56$^{\#}$	48.31 ± 2.7$^{\#}$	20.21 ± 1.6$^{\#}$	7.29
KTZ-SLNs	6643.67 ± 309.16*	134.40 ± 4.2*	45.90 ± 2.3*	16.52

*Indicates a difference between KTZ-SLNs and other groups (KTZ-SUS and KTZ-MKT); $p < 0.05$

$^{\#}$Indicates a difference between KTZ-MKT and KTZ-SUS; $p < 0.05$

Table 4 In vivo dermatokinetic parameters of KTZ-SLNs, KTZ-MKT, and KTZ-SUS following topical application to rat skin (mean ± SD, $n = 6$)

Formulation	C_{max} (µg/mL)	T_{max} (h)	$AUC_{0-\infty}$ (µg h/mL)	$AUMC_{0-\infty}$ (µg h^2/mL)
KTZ-SUS	31.71 ± 3.5	24	1105.33 ± 118.7	42,149.12 ± 1601.7
KTZ-MKT	55.09 ± 3.5*	24	2146.22 ± 176.5*	80,288.69 ± 4301.6*
KTZ-SLNs	225.19 ± 9.5#	24	9901.77 ± 429.6#	448,892.14 ± 2918.9#

#Indicates a difference between KTZ-SLNs and other groups; $p < 0.001$

*Indicates a difference between KTZ-MKT and KTZ-SUS; $p < 0.001$

that KTZ, if any, was present at concentration below lower limit of detection (LLOD) of 0.2 µg/mL. It may be prudent to correlate mitigated systemic toxicity and drug related side effects of KTZ as compared to its oral or parenteral administration [52].

The achieved high permeation potential of KTZ-SLNs is attributed to a combination of mechanisms functioning together, such as (a) surfactant- and lipid-mediated cellular internalization of the KTZ through skin lamellar lipid, (b) increased surface area maximized drug availability around fungal cells, (c) reduced particle size caused ease in permeation across microscopic physiological pores, (d) lipid-based bioadhesion and subsequent thin film formation protected dehydration of skin, and (e) slow and controlled access of the drug to the targeted epidermal area provided regular exposure of fungal strains with the drug.

Fluorescence microscopy study

To support the ex vivo permeation and drug deposition findings, this study was planned to visualize the dye-loaded SLNs (FL-SLNs) applied on human dermatomed skin for 2 and 24h under fluorescent microscopy. An aqueous solution of the dye served as control and was applied on the same skin. The fluorescent images are shown in Fig. 9. From Fig. 9A and B, the fluorescence was only detected at the skin surface in the fluorescein solution group after cultivation for 2h and 24h. Fluorescence displayed only little penetration from external epidermis layer after 2h treatment (Fig. 9C) with fluorescein-loaded in SLNs. After 24h of treatment, FL-SLN treatment group showed appreciable fluorescence deeper inside the viable epidermis (Fig. 9D).

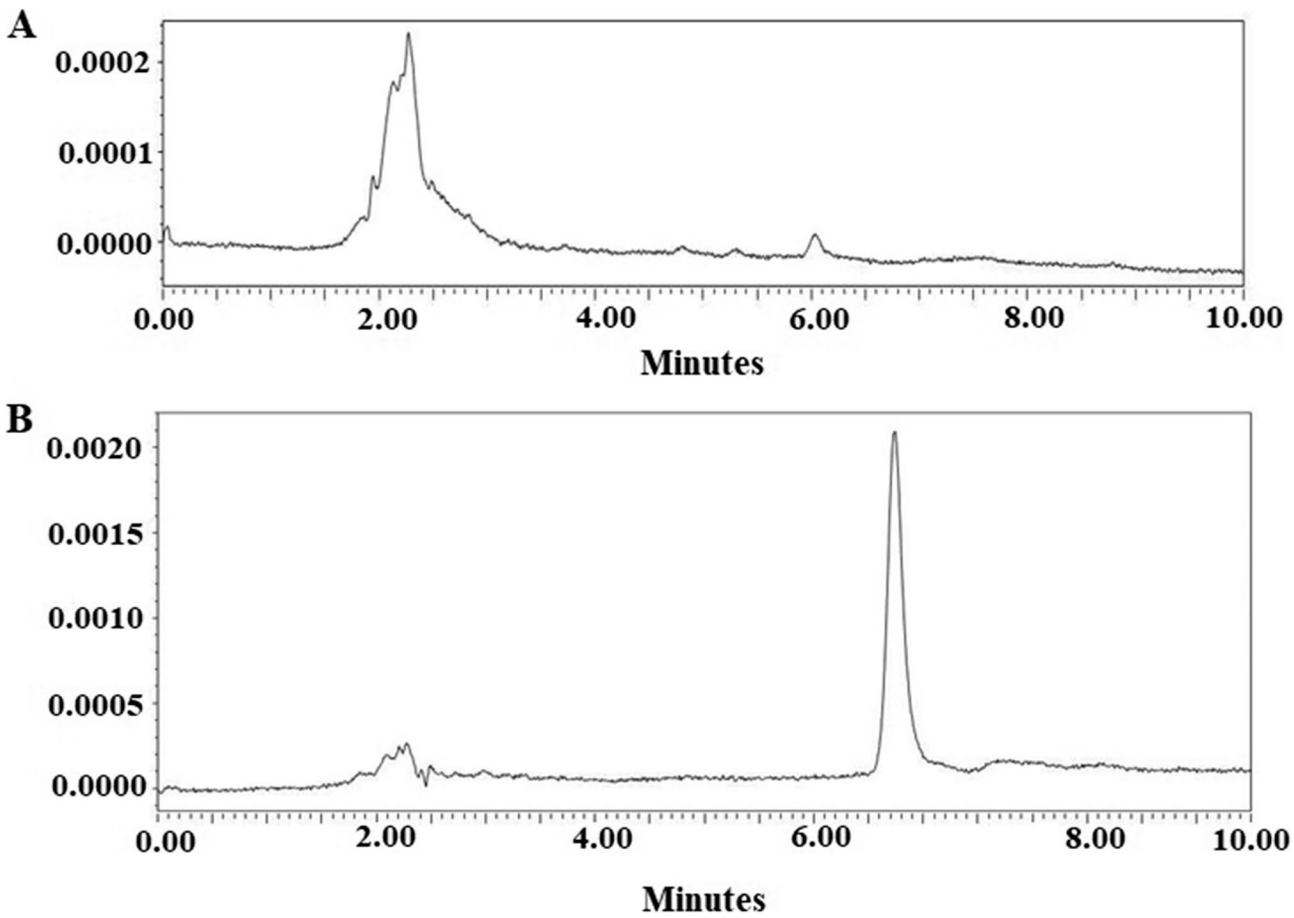

Fig. 8 HPLC chromatograms of (**A**) blank skin homogenate and (**B**) KTZ in skin homogenate

SLNs are reported to permeate the skin where they are found to accumulate resulting in a depot, and subsequent release of KTZ from SLNs present in skin/hair follicles will provide an effective, sustained treatment of fungal infection [41, 47].

Vibrational spectroscopy imaging of human skin

ATR-FTIR imaging on skin cross-section

Human skin cross-sections were recorded by ATR-FTIR imaging spectroscopy. Figure 10 shows visible images of a skin cross-section and the associated hyperspectral image. The method allowed us to investigate and visualize the penetration of KTZ-loaded KTZ-SLNs and other SLN components in the integral epidermis.

The FTIR Imaging System recorded hyperspectral images (Fig. 11) which provide maps showing the co-localization of specific molecular components (KTZ or SLN components). These images were generated with false colours where the red represents the highest values and the blue the lowest values for each parameter investigated. The ratio between 816 cm^{-1} and Amide I band area was used to follow the penetration of KTZ while the ratio between 945 cm^{-1} and Amide I band area was used to follow the penetration of SLN components. Indeed, the band around 816 cm^{-1} is specific of the KTZ while the band around 945 cm^{-1} is specific of the SLN components. There is no overlapping with the skin contribution in this area (Supplementary Fig. 1). The typical FTIR spectra recorded on KTZ-SLNs and on untreated human skin, shown in this figure, were used to define the IR markers for the KTZ and for the SLNs. The ratios used to investigate the penetration of KTZ and SLNs were applied to the three skin groups: untreated, treated 3 and 24h with KTZ-SLNs and the data shown in Fig. 11 (FTIR results) and Fig. 12 below (Raman results) present, in our opinion, clear results regarding the penetration of KTZ inside human skin samples as well as the penetration of the SLNs. As expected, using these ratios no KTZ neither SLN penetration can be observed in the untreated human skin samples in both FTIR and Raman experiments. Hyperspectral images in Figs. 10 and 11 show clearly that KTZ and SLNs penetrated inside the human skin, and the deepest penetration was reached after 24h of treatment. This is a first report where such spectral studies are used to describe penetration of any SLN formulation into human skin.

The SLN penetration will allow the release of KTZ inside the human skin samples when they will exhibit polymorphic transition from β to β' a more stable crystalline form [35]. The ATR-FTIR images in the Supplementary Fig. 2 show clearly that SLNs penetrated inside the human skin, and the maximum penetration was reached after 24h of treatment. After 24h, the SLNs had penetrated up to the deepest part of the epidermis.

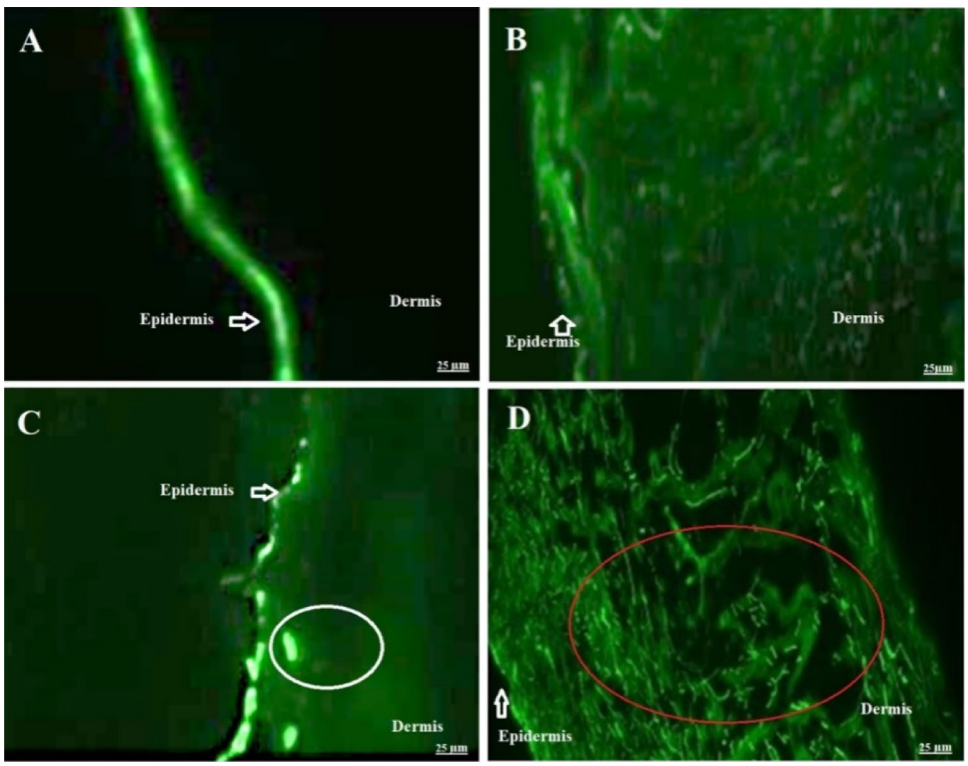

Fig. 9 Fluorescent images of skin tissue. (**A**) FL-Sol 2h, (**B**) FL-Sol 24h, (**C**) FL-SLNs 2h, (**D**) FL-SLNs 24h

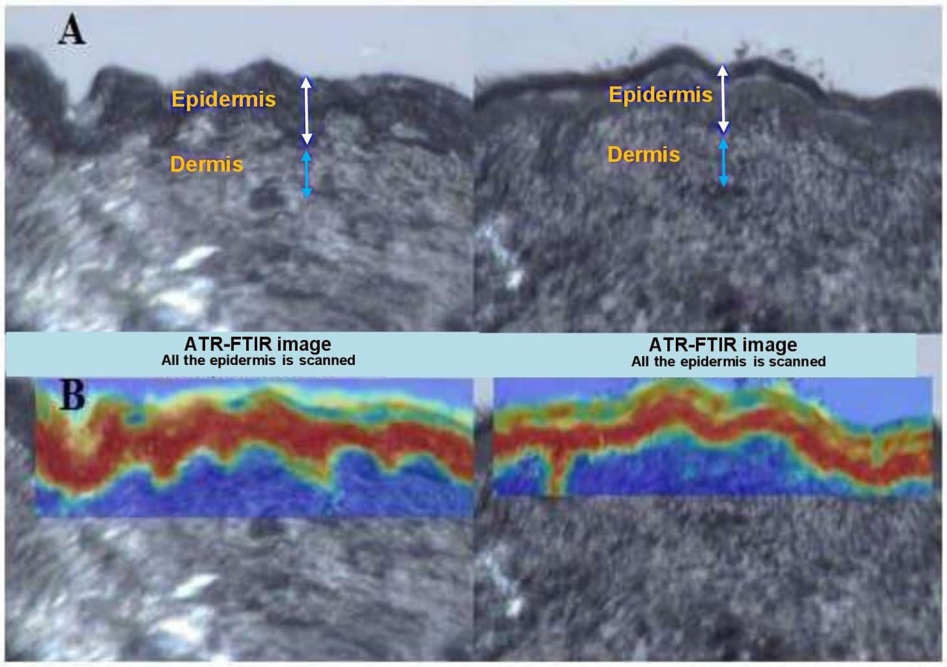

Fig. 10 (**A**) Visible image of skin cross-section showing the epidermis and dermis region. (**B**) Hyperspectral FTIR images superimposed on the visible image indicating the whole epidermis was scanned

Confocal Raman spectroscopy imaging

The FTIR data were confirmed by confocal Raman spectroscopy. The confocal Raman images in Fig. 12 clearly show that SLNs penetrated the stratum corneum in the first 2h and reached the viable epidermis after 24h. There was a nice co-localization of the KTZ and the SLNs inside the human skin samples. Indeed, like the SLNs the KTZ penetrated the stratum corneum in the first 2h and reached the deeper part of the epidermis after 24h.

Long-term stability

Nanoparticles are associated with instability due to physical and chemical factors such as particulate aggregation, size variation, and drug content under varied temperature and

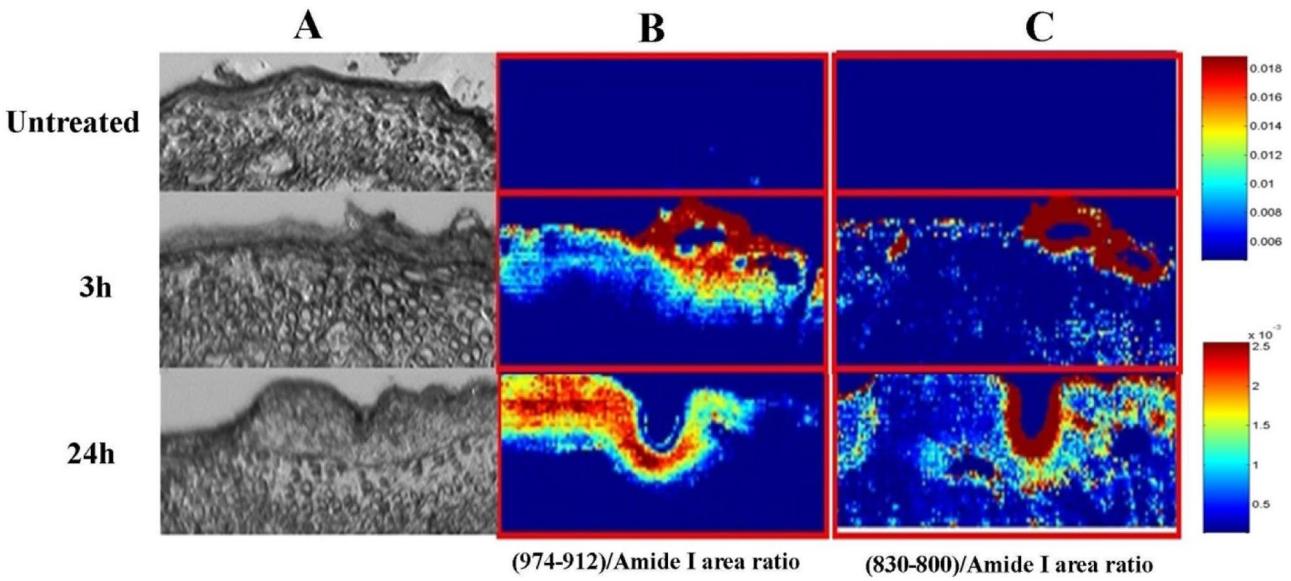

Fig. 11 (**A**) Visible images of skin cross-sections (stratum corneum on the top) (**B**) ATR-FTIR image of KTZ-SLN penetration into the skin, obtained from the ratio between 945 cm^{-1} and Amide I peak area (representative of SLN components) and (**C**) ATR-FTIR image of KTZ-SLN penetration into the skin, obtained from the ratio of the peak areas at 816 cm^{-1} to Amide I (representative of KTZ) peak area. Highest to lowest concentration of each component is displayed by the colour scale from red (highest) to blue (lowest) as shown

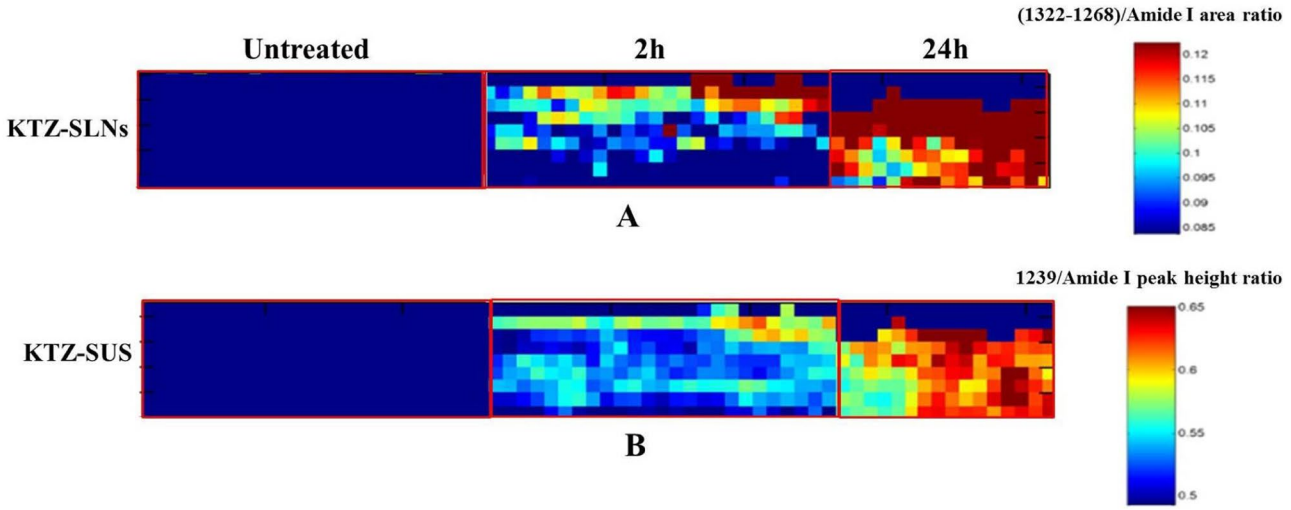

Fig. 12 Confocal Raman images showing that SLNs have penetrated inside human skin treated with (**A**) KTZ-SLNs and (**B**) KTZ-SUS for 2h and 24h. Highest to lowest concentration of each component is displayed by the colour scale from red (highest) to blue (lowest/no component) as shown

humidity. Therefore, it is an essential parameter to estimate shelf life of a product or success of the product to comply regulatory condition before approval or marketing. Particle size (PS), % EE, and the drug content were estimated over different temperature, humidity, and time period as shown in Fig. 13. The PS of KTZ-SLN stored at 4 °C ± 1.0 °C (2-8°C), 30 °C ± 2 °C/65 ± 5% RH, and 40 °C ± 2 °C/75 ± 5%RH ranged as 236.8 ± 16.7–565.2 ± 20.5 nm, 336.8 ± 16.7–658.7 ± 98.5, and 336.8 ± 16.7–1346.98 ± 133.1 respectively. Particle growth was slower at 4 ± 1.0 °C than when stored at higher temperatures. Kinetic energy of the system increases at higher temperatures, yielding aggregates (and hence increase in size)

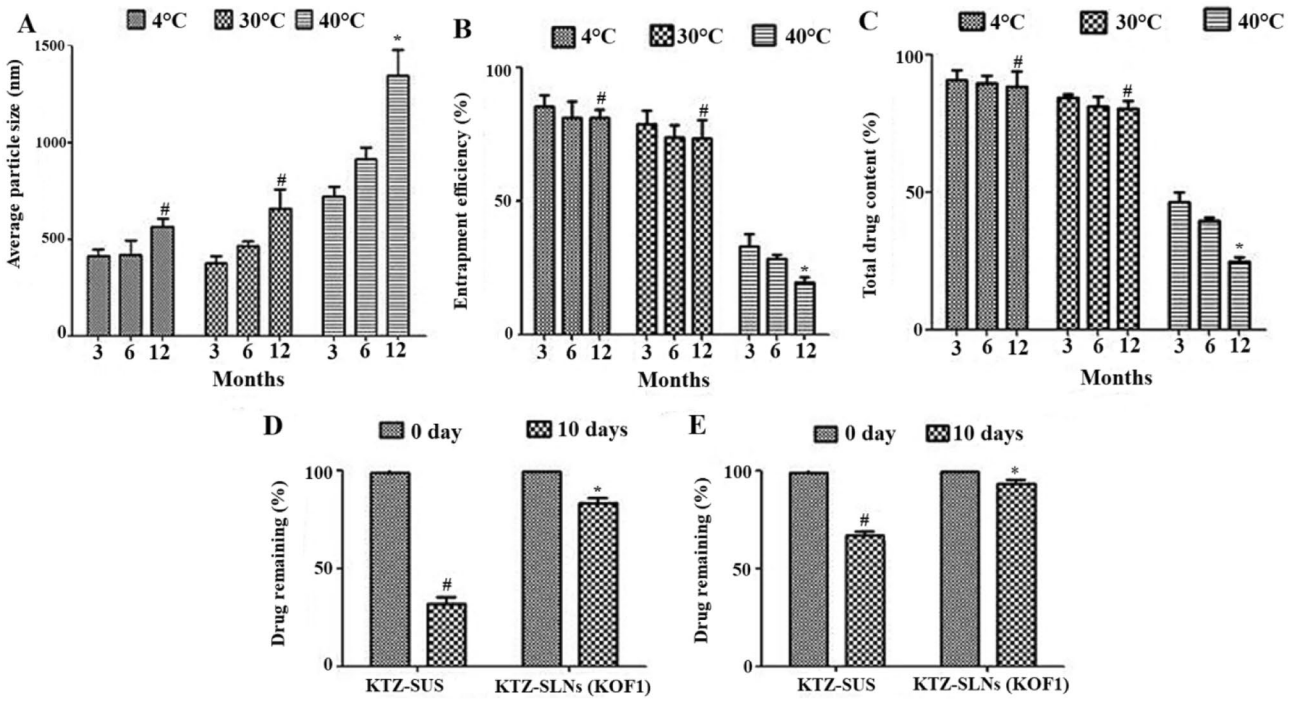

Fig. 13 Effect of different temperatures on particle size (**A**), %EE (**B**), and % total drug content (**C**) in long-term stability studies. Effect of UV light on KTZ-SLNs (KOF1) and KTZ-SUS in amber-coloured glass (**D**) and transparent glass (**E**)

due to higher frequency of collisions between particles [53, 54]. Microviscosity (the friction experienced by particles) is a temperature-dependent factor and decreases with an increase in temperature leading to particle destabilization and possibly agglomeration [55]. The %EE of KTZ-SLNs stored at 4 °C ± 1.0 °C (2-80 C), 30 °C ± 2 °C/65% RH ranged between 87.5 ± 3.2–81.2 ± 0.7% and 87.5 ± 3.2–73.5 ± 1.9% respectively. The corresponding drug assay (%TDC) for KTZ-SLNs ranged between 94.9 ± 1.7 and 87.90 ± 0.6% and between 94.9 ± 1.7 and 80.5 ± 0.8%, respectively. The %EE and %TDC of KTZ-SLNs stored at 40 °C ± 2 °C/75% RH ± 5% RH ranged between 87.5 ± 3.2–19.3 ± 1.1% and 94.9 ± 1.7–24.92 ± 1.7% respectively. The chromatograms of stability did not show any interference of degradation products. Further peak purity values were from 99.67 to 99.86 for all stability samples and the same RT of KTZ in all samples confirmed that degradation products did not interfere with the KTZ peak (results not shown). High temperatures (40 ± 2 °C/75 ± 5% RH) facilitate transformation of lipid into various metastable polymorphic states which results in drug expulsion and leaching. A transformation of SLN from β' to β form resulting in drug expulsion is indicated by significantly decreased EE [56]. The investigated drug is also associated with light-mediated instability. Interestingly, the total drug content (%TDC) was found to be reduced under UV light ($p < 0.05$; Fig. 13D and E) in drug suspension at the end of 10 days. In contrast, %TDC remained substantially high in SLNs at the end of 10 days. KTZ-SUS showed a significant ($p < 0.001$) reduction in %TDC (remaining drug as 66.4%) when stored in the transparent glass vial as compared to amber glass (remaining drug content as 30.3%). This was also inspected for visual examination. The drug content stored in transparent glass turned to slightly pink colour upon storage (suspension) whereas KTZ-SLNs retained their white colour. This may be prudent to correlate with high protective nature of Compritol possessing low peroxide value as mentioned before [13].

Conclusions

KTZ is a potential established antifungal drug with limited aqueous solubility and poor topical efficacy in conventional dosage form. Commercial cream available is also challenged for limited clinical efficacy on topical application to control resistant and recurrence cases. In literature, various topical and transdermal formulations have been reported for improved efficacy based on overestimated data of in vitro findings. Therefore, we addressed solid lipid nanoparticle with optimum level of Compritol and tween 80 to achieve desired size, %EE, and %TDC. Ex vivo permeation and drug deposition findings were further supported with fluorescence microscopy study using dermatome human skin model after topical application. It was important to investigate and assess in a human skin model for mechanistic and tangible degree of permeation across the crystalline barrier (stratum corneum). Moreover, in vivo dermatokinetics data assured that the SLN was capable to carry the drug to the deeper layer of the epidermal region in substantial concentration with limited transport to systemic circulation. Vibrational imaging spectroscopy techniques was used as proof of concept and KTZ-SLNs were confirmed to penetrate up to the viable epidermis human skin. Finally, long-term stability and photostability data indicated protective benefits of Compritol used in the formulation. Thus, the Compritol-based SLN was a promising carrier for improved permeation, drug deposition, penetration, dermatokinetics parameters, and increased stability over long period.

Supplementary Information The online version contains supplementary material available at https://doi.org/10.1007/s13346-021-01058-6.

Acknowledgements The authors acknowledge the UGC-CAS, DST-FIST, and PURSE funded facility of UIPS, Panjab University, India used for characterization of KTZ-SLNs; SAIF facility of DST at Panjab University Chandigarh, India; TRI Princeton and Centre for Dermal Research, New Jersey, USA for conduct of permeation studies; and ATR-FTIR and Confocal Raman spectroscopy studies.

Author contribution Mohhammad Ramzan: conduct of experiments, manuscript writing and drafting; Samuel Gourion-Arsiquaud: permeation studies using vibrational spectroscopy, review and editing; Afzal Hussain: manuscript editing and review; Jaspreet Singh Gulati: supply of materials, study protocol; Qihong Zhang: vibrational spectroscopic studies; Sonia Trehan: fluorescent microscopic studies and discussions between collaborating groups; Vinam Puri: analytical method development; Bozena Michniak-Kohn: collaboration between teams of various Institutes, manuscript reviewing. Indu Pal Kaur: experimental protocol design, conceptualization, review and editing.

Funding UGC-RFSMS, University Grants Commission, New Delhi. BT/SBIRI/1744/FF funding grant from BIRAC-DBT, New Delhi, India is highly acknowledged.

Availability of data and materials NA.

Declarations

Ethics approval and consent to participate All animal experiments are conducted after ethical approval from the Institutional Animal Ethics Committee of Panjab University, Chandigarh (PU/45/99/CPCSEA/IAEC/2018/150). The procedure adopted for the in vivo studies was as per ARRIVE guidelines.

Consent for publication All of the authors agreed with the content and gave explicit consent to submit the work.

Competing interests The authors declare no competing interests.

References

1. Hainer BL. Dermatophyte infections. Am Fam Physician. 2003;67:101–8.
2. Ameen M. Epidemiology of superficial fungal infections. Clin Dermatol. 2010;28:197–201.

3. Kyle AA, Dahl MV. Topical therapy for fungal infections. Am J Clin Dermatol. 2004;5:443–51.
4. Kühbacher A, Burger-Kentischer A, Rupp S. Interaction of Candida species with the skin. Microorganisms. 2017;5:32.
5. Holmes AR, Cardno TS, Strouse JJ, Ivnitski-Steele I, Keniya MV, Lackovic K, Monk BC, Sklar LA, Cannon RD. Targeting efflux pumps to overcome antifungal drug resistance. Future Med Chem. 2016;8:1485–501.
6. Choi FD, Juhasz ML, Mesinkovska NA. Topical ketoconazole: a systematic review of current dermatological applications and future developments. J Dermatolog Treat. 2019;30:760–71.
7. Logua AD, Faddab AM, Anchisib C, Maccionib AM, Sinicob C, Schivoa ML, Alhaiquec F. Effects of in-vitro activity of miconazole and ketoconazole in phospholipid formulations. J Antimicrob Chemother. 1997;40:889–93.
8. FDA. Drug Safety Podcast. 2010. https://www.fda.gov/Drugs/DrugSafety/DrugSafetyPodcasts/ucm504300.htm. Acesssed 09 Nov 2020.
9. Guo F, Wang J, Ma M, Tan F, Li N. Skin targeted lipid vesicles as novel nano-carrier of ketoconazole: characterization in vitro and in vivo evaluation. J Mater Sci Mater Med. 2015;26:175.
10. Nayak D, Tawale RM, Aranjani JM, Tippavajhala VK. Formulation, optimization and evaluation of novel ultra-deformable vesicular drug delivery system for an anti-fungal drug. AAPS Pharm Sci Tech. 2020;21:140.
11. Mahtab A, Anwar M, Mallick N, Naz Z, Jain GK, Ahmad FJ. Transungual delivery of ketoconazole nanoemulgel for the effective management of onychomycosis. AAPS Pharm Sci Tech. 2016;17:1477–90.
12. Hussain A, Alshehri S, Ramzan M, Afzal O, Altamimi ASA, Alossaimi MA. Biocompatible solvent selection based on thermodynamic and computational solubility models in-silico GastroPlus prediction and cellular studies of ketoconazole for subcutaneous delivery. J Drug Deliv Sci Technol. 2021;65:102699.
13. Souto EB, Müller RH. SLN and NLC for topical delivery of ketoconazole. J Microencapsul. 2005;22:501–10.
14. Dave V, Sharma S, Yadav RB, Agarwal U. Herbal liposome for the topical delivery of ketoconazole for the effective treatment of seborrheic dermatitis. Appl Nanosci. 2017;7:973–87.
15. Wolf M, Halper M, Pribyl R, Baurecht D, Valenta C. Distribution of phospholipid based formulations in the skin investigated by combined ATR-FTIR and tape stripping experiments. Int J Pharm. 2017;519:198–205.
16. Binder L, Kulovits EM, Petz R, Ruthofer J, Baurecht D, Klang V, Valenta C. Penetration monitoring of drugs and additives by ATR-FTIR spectroscopy/tape stripping and confocal Raman spectroscopy – a comparative study. Eur J Pharm Biopharm. 2018;130:214–23.
17. Ramzan M, Kaur G, Trehan S, Agrewala JN, Michniak-Kohn BB, Hussain A, Mahdi WA, Gulati JS, Kaur IP. Mechanistic evaluations of ketoconazole lipidic nanoparticles for improved efficacy enhanced topical penetration cellular uptake (L929 and J774A.1) and safety assessment: in vitro and in vivo studies. J Drug Deliv Sci Technol. 2021;65:102743.
18. Sharma G, Chopra K, Puri S, Bishnoi M, Rishi P, Kaur IP. Topical delivery of TRPsiRNA-loaded solid lipid nanoparticles confer reduced pain sensation via TRPV1 silencing in rats. J Drug Target. 2018;26:135–49.
19. Ramasamy T, Khandasami US, Ruttala H, Shanmugam S. Development of solid lipid nanoparticles enriched hydrogels for topical delivery of anti-fungal agent. Macromol Res. 2012;20:682–92.
20. Kakkar S, Karuppayil SM, Raut JS, Giansanti F, Papucci L, Schiavone N, Kaur IP. Lipid-polyethylene glycol based nano-ocular formulation of ketoconazole. Int J Pharm. 2015;495:276–89.
21. Dudhipala N, Ay AA. Amelioration of ketoconazole in lipid nanoparticles for enhanced antifungal activity and bioavailability through oral administration for management of fungal infections. Chem Phys Lipids. 2020;232:104953.
22. Carbone C, Fuochi V, Zielińska A, Musumeci T, Souto EB, Bonaccorso A, Puglia C, Petronio Petronio G, Furneri PM. Dual-drugs delivery in solid lipid nanoparticles for the treatment of *Candida albicans* mycosis. Colloids Surf B. 2020;186:110705.
23. Patil PR, Biradar SV, Paradkar AR. Extended release felodipine self-nanoemulsifying system. AAPS Pharm Sci Tech. 2009;10:515–23.
24. Kaur IP, Kakkar S, Singla A, inventors. Nanostructured lipidic polymeric pharmaceutical compositions encapsulating drugs. (Indian patent 336184) 2020.
25. Alshehri S, Hussain A, Ahsan MN, Ali R, Siddique MUM. Thermodynamic, computational solubility parameters in organic solvents and in silico gastroplus based prediction of ketoconazole. ACS Omega. 2021;6:5033–45.
26. Das S, Ng WK, Kanaujia P, Kim S, Tan RBH. Formulation design, preparation and physicochemical characterizations of solid lipid nanoparticles containing a hydrophobic drug: effects of process variables. Colloids Surf B. 2011;88:483–9.
27. Hu L, Tang X, Cui F. Solid lipid nanoparticles (SLNs) to improve oral bioavailability of poorly soluble drugs. J Pharm Pharmacol. 2004;56:1527–35.
28. Hussain A, Samad A, Nazish I, Ahmed FJ. Nanocarrier-based topical drug delivery for an antifungal drug. Drug Dev Ind Pharm. 2014;40:527–41.
29. Zhang Q, Murawsky M, LaCount T, Hao J, Kasting GB, Newman B, Ghosh P, Raney SG, Li SK. Characterization of temperature profiles in skin and transdermal delivery system when exposed to temperature gradients in vivo and in vitro. Pharm Res. 2017;34:1491–504.
30. Barry BW. Mode of action of penetration enhancers in human skin. J Control Release. 1987;6:85–97.
31. Abioye AO, Issah S, Kola-Mustapha AT. Ex vivo skin permeation and retention studies on chitosan–ibuprofen–gellan ternary nanogel prepared by in situ ionic gelation technique—a tool for controlled transdermal delivery of ibuprofen. Int J Pharm. 2015;490:112–30. https://doi.org/10.1016/j.ijpharm.2015.05.030.
32. ICH. Q1B photostability testing of new drug substances and products. https://www.fda.gov/regulatory-information/search-fda-guidance-documents/q1b-photostability-testing-new-drug-substances-and-products. Accessed on 12 Feb 2020.
33. ICH. Q1A (R2) Stability testing of new drug substances and products. https://www.fda.gov/regulatory-information/search-fda-guidance-documents/q1ar2-stability-testing-new-drug-substances-and-products. Accessed on 25 Feb 2021.
34. Aburahma MH, Badr-Eldin SM. Compritol 888 ATO: a multifunctional lipid excipient in drug delivery systems and nanopharmaceuticals. Expert Opin Drug Deliv. 2014;11:1865–83.
35. Souto EB, Mehnert W, Müller RH. Polymorphic behaviour of Compritol®888 ATO as bulk lipid and as SLN and NLC. J Microencapsul. 2006;23:417–33.
36. Muller RH, Runge S, Ravelli V, Mehnert W, Thunemann AF, Souto EB. Oral bioavailability of cyclosporine: solid lipid nanoparticles (SLN®) versus drug nanocrystals. Int J Pharm. 2006;317:82–9.
37. Karolewicz B, Górniak A, Owczarek A, Żurawska-Płaksej E, Piwowar A, Pluta J. Thermal spectroscopic and dissolution studies of ketoconazole–Pluronic F127 system. J Therm Anal Calorim. 2014;115:2487–93.
38. Tatke A, Dudhipala N, Janga KY, Balguri SP, Avula B, Jablonski MM, Majumdar S. In situ gel of triamcinolone acetonide-loaded

solid lipid nanoparticles for improved topical ocular delivery: tear kinetics and ocular disposition studies. Nanomaterials. 2018;9:33.
39. Vieira IRS, Miranda GdS, Ricci-Júnior E, Delpech MC. Waterborne poly(urethane-urea)s films as a sustained release system for ketoconazole. Polymers. 2019;19:168–80.
40. Vasoya J, Shah A, Serajuddin A. Investigation of possible solubility and dissolution advantages of cocrystals I: aqueous solubility and dissolution rates of ketoconazole and its cocrystals as functions of pH. ADMET DMPK. 2019;7:106.
41. Deng P, Teng F, Zhou F, Song Z, Meng N, Liu N, Feng R. Y-shaped methoxy poly (ethylene glycol)-block-poly (epsilon-caprolactone)-based micelles for skin delivery of ketoconazole: in vitro study and in vivo evaluation. Mater Sci Eng C. 2017;78:296–304.
42. Jores K, Mehnert W, Drechsler M, Bunjes H, Johann C, Mäder K. Investigations on the structure of solid lipid nanoparticles (SLN) and oil-loaded solid lipid nanoparticles by photon correlation spectroscopy, field-flow fractionation and transmission electron microscopy. J Control Release. 2004;95:217–27.
43. de Jesus MB, Zuhorn IS. Solid lipid nanoparticles as nucleic acid delivery system: Properties and molecular mechanisms. J Control Release. 2015;201:1–13.
44. Fu Y, Kao WJ. Drug release kinetics and transport mechanisms of non-degradable and degradable polymeric delivery systems. Expert Opin Drug Deliv. 2010;7:429–44.
45. Wissing SA, Müller RH. Cosmetic applications for solid lipid nanoparticles (SLN). Int J Pharm. 2003;254:65–8.
46. Sabir F, Qindeel M, Rehman Au, Ahmad NM, Khan GM, Csoka I, Ahmed N. An efficient approach for development and optimisation of curcumin-loaded solid lipid nanoparticles' patch for transdermal delivery. J Microencapsul. 2021;38:233–48.
47. Knorr F, Lademann J, Patzelt A, Sterry W, Blume-Peytavi U, Vogt A. Follicular transport route–research progress and future perspectives. Eur J Pharm Biopharm. 2009;71:173–80.
48. Jensen LB, Petersson K, Nielsen HM. In vitro penetration properties of solid lipid nanoparticles in intact and barrier-impaired skin. Eur J Pharm Biopharm. 2011;79:68–75.
49. Chen H, Chang X, Du D, Liu W, Liu J, Weng T, Yang Y, Xu H, Yang X. Podophyllotoxin-loaded solid lipid nanoparticles for epidermal targeting. J Control Release. 2006;110:296–306.
50. Hussain A, Singh SK. Evidences for anti-mycobacterium activities of lipids and surfactants. World J Microbiol Biotechnol. 2015;32:7.
51. Hussain A, Samad A, Singh SK, Ahsan MN, Faruk A, Ahmed FJ. Enhanced stability and permeation potential of nanoemulsion containing sefsol-218 oil for topical delivery of amphotericin B. Drug Dev Ind Pharm. 2015;41:780–90.
52. Sugar AM, Alsip SG, Galgiani JN, Graybill JR, Dismukes WE, Cloud GA, Craven PC, Stevens DA. Pharmacology and toxicity of high-dose ketoconazole. Antimicrob Agents Chemother. 1987;31:1874–8.
53. Hu F-Q, Jiang S-P, Du Y-Z, Yuan H, Ye Y-Q, Zeng S. Preparation and characteristics of monostearin nanostructured lipid carriers. Int J Pharm. 2006;314:83–9.
54. Wissing SA, Kayser O, Müller RH. Solid lipid nanoparticles for parenteral drug delivery. Adv Drug Deliv Rev. 2004;56:1257–72.
55. Heurtault B, Saulnier P, Pech B, Proust J-E, Benoit J-P. Physico-chemical stability of colloidal lipid particles. Biomaterials. 2003;24:4283–300.
56. Das S, Ng WK, Tan RBH. Are nanostructured lipid carriers (NLCs) better than solid lipid nanoparticles (SLNs): development, haracterizations and comparative evaluations of clotrimazole-loaded SLNs and NLCs? Eur J Pharm Sci. 2012;47:139–51.